Title
Micro and Nano Interdigitated Electrode Array (IDEA)-Based MEMS/NEMS as Electrochemical Transducers: A Review

Journal
Nanomaterials, 12(23)

ISSN
2079-4991

Authors
Kosri, Elyana
Ibrahim, Fatimah
Thiha, Aung
et al.

Publication Date
2022

DOI
10.3390/nano12234171

nanomaterials

MDPI

Review

Micro and Nano Interdigitated Electrode Array (IDEA)-Based MEMS/NEMS as Electrochemical Transducers: A Review

Elyana Kosri [1,2], Fatimah Ibrahim [1,2,3,*], Aung Thiha [1,2] and Marc Madou [2,4,5,6]

[1] Department of Biomedical Engineering, Faculty of Engineering, Universiti Malaya, Kuala Lumpur 50603, Malaysia
[2] Centre for Innovation in Medical Engineering (CIME), Faculty of Engineering, Universiti Malaya, Kuala Lumpur 50603, Malaysia
[3] Centre of Printable Electronics, Universiti Malaya, Kuala Lumpur 50603, Malaysia
[4] Department of Mechanical and Aerospace Engineering, University of California Irvine, Irvine, CA 92697, USA
[5] School of Engineering and Sciences, Tecnologico de Monterrey, Monterrey 64849, NL, Mexico
[6] Academia Mexicana de Ciencias, Ciudad de México 14400, CDMX, Mexico
* Correspondence: fatimah@um.edu.my

Abstract: Micro and nano interdigitated electrode array (μ/n-IDEA) configurations are prominent working electrodes in the fabrication of electrochemical sensors/biosensors, as their design benefits sensor achievement. This paper reviews μ/n-IDEA as working electrodes in four-electrode electrochemical sensors in terms of two-dimensional (2D) planar IDEA and three-dimensional (3D) IDEA configurations using carbon or metal as the starting materials. In this regard, the enhancement of IDEAs-based biosensors focuses on controlling the width and gap measurements between the adjacent fingers and increases the IDEA's height. Several distinctive methods used to expand the surface area of 3D IDEAs, such as a unique 3D IDEA design, integration of mesh, microchannel, vertically aligned carbon nanotubes (VACNT), and nanoparticles, are demonstrated and discussed. More notably, the conventional four-electrode system, consisting of reference and counter electrodes will be compared to the highly novel two-electrode system that adopts IDEA's shape. Compared to the 2D planar IDEA, the expansion of the surface area in 3D IDEAs demonstrated significant changes in the performance of electrochemical sensors. Furthermore, the challenges faced by current IDEAs-based electrochemical biosensors and their potential solutions for future directions are presented herein.

Keywords: interdigitated electrode array; carbon MEMS; cyclic voltammetry; electrochemical analysis; nanocomposites; nanoparticles; electrochemical transducer; biosensor

Citation: Kosri, E.; Ibrahim, F.; Thiha, A.; Madou, M. Micro and Nano Interdigitated Electrode Array (IDEA)-Based MEMS/NEMS as Electrochemical Transducers: A Review. *Nanomaterials* **2022**, *12*, 4171. https://doi.org/10.3390/nano12234171

Academic Editor: Run Zhang

Received: 19 October 2022
Accepted: 15 November 2022
Published: 24 November 2022

1. Introduction

A biosensor typically consists of three main elements, namely a bioreceptor, transducer, and signal processing system [1]. A bioreceptor, also known as biological recognition element, involves an immobilized biocomponent, which is capable of detecting a specific target analyte [2]. Nucleic acid, enzymes, antibodies, cells, etc., are types of biocomponents. A transducer is a converter that converts a biochemical signal into an electrical signal [3]. The reaction between a bioreceptor and target analytes generates distinct chemical reactions, such as electron flow, release of heat, and changes in pH or mass, subsequently creating new chemicals. The detection of an electrical signal by the transducer is amplified and sent to microelectronics and data processors for signal measurement in terms of a print out, an optical change, or as digital display. Biosensors can be categorized into bioreceptors and transducers. Bioreceptors consist of biomimetics, enzymes, phages, DNA, cells, and antibodies. The transducer can be further divided into three categories, which are: (i) those based on electrochemical transducers, such as electrical impedance spectroscopy (EIS), potentiometric, amperometric, and conductometric; (ii) mass-based, such as piezoelectric and magnetoelastic; and (iii) optical-based biosensors, such as chemiluminescence, fluorescence,

surface plasmon resonance (SPR), fibre optic, and others. The classification of biosensors has been described in several pieces of literature and is illustrated in Figure 1 [4–6].

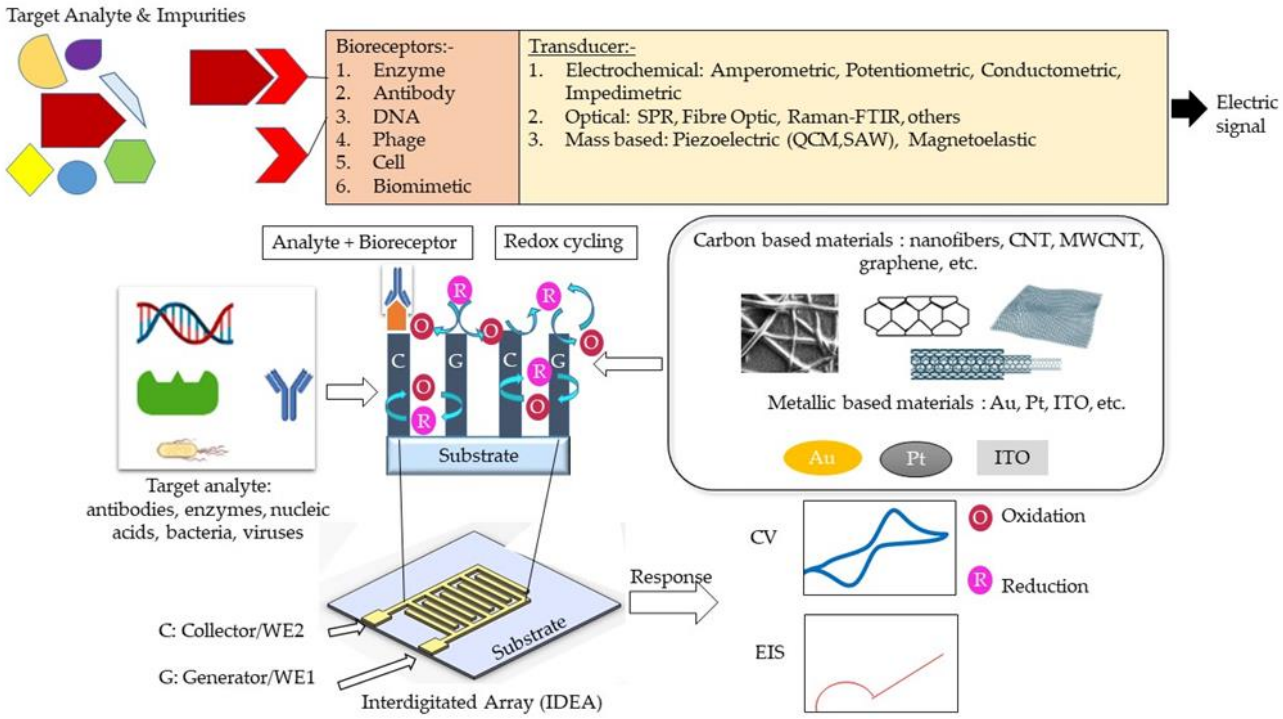

Figure 1. Schematic design of IDEA design-based electrochemical detection (amperometric and impedimetric) methods.

The electrochemical biosensing techniques can be divided into amperometric, impedimetric, conductometric, and potentiometric sensing [5]. In an amperometric sensor, one measures the current response at a fixed potential to detect the concentration of an analyte [7]. In a potentiometric sensor, potential changes at a working/sensing electrode are measured with respect to a reference electrode and under the conditions of constant current (i.e., typically zero). Conductometric sensors measure the electrolytic conductivity to monitor the progress of a reaction. An impedimetric sensor works by measuring an impedance change while applying a small sinusoidal voltage that is varied over a range of frequencies. Electrochemical sensors are among the most popular biosensors due to their simplicity, good-to-excellent limit of detection (LOD), high selectivity, and ease of fabrication, as well as the promising opportunity for miniaturization and low-cost fabrication [6,8–10]. Innovative electrodes in electrochemical cells can be mass-manufactured using a variety of materials and economical manufacturing processes [11–13]. Moreover, integrated circuit technologies make it possible to integrate electrodes with electronics for further biosensor miniaturization [14,15].

A basic electrochemical three-electrode cell consists of a working electrode, a counter electrode, and a reference electrode. The working electrode is the actual transduction element for the electrochemical reaction at the electrode/analyte solution interface. A current at the working electrode is offset by an equal but opposite current at the counter electrode, and hence there is no current flow between the working and high-input impedance reference electrode, allowing us to accurately track changes in the working electrode potential. The counter electrode must be of large surface area (since the current through the cell must be controlled by the reaction at the working electrode) with a stable and good conductor [16]. Carbon [17], platinum (Pt) [18], gold (Au) [19], and other materials [7,20,21] are the common materials used to fabricate the counter electrode. Reference electrodes are designed so that an equilibrium is set up with a known potential between a metal wire and

the surrounding solution. A silver/silver chloride (Ag/AgCl) system is widely used as a reference electrode [22,23].

Despite the booming interests in IDEAs that started more than 30 years ago, current studies manipulate materials from different sources to suit the electrode usage of IDEA. Interdigitated electrode array (IDEA) from carbon and metal sources, in contrast, emerges as a favorable electrode biosensor for various health-monitoring and biomedical applications. Indeed, numerous pieces of research highlighting the development of an IDEAs-based biosensor with various detection methods have been extensively reported [24–26]. Enhanced signal amplification allowing detection of low-concentration bioanalytes displayed by an IDEAs-based biosensor proved to be advantageous for electrochemical biosensing [27–29]. With an IDEA configuration, the limit of detection (LOD) of a biosensor can be significantly improved [30]. In such a configuration, two comb-shaped working electrodes are arranged in an interdigitated manner, as presented in Figure 1 [31,32]. IDEAs are widely used as impedimetric transducers in electrochemical impedance spectroscopy (EIS) [33–35]. EIS employs a controlled alternating current (AC) with electrical stimulus between 5 and 10 mV to measure small variations in capacitance/resistance caused by analyte and electrode surface interactions. These capacitance and resistance changes are due to changes in faradaic (electron transfer/resistance changes) and non-faradaic (dielectric/capacitance changes) processes at the electrode surface [36]. The signal strength of an IDEA-based biosensor can be controlled through the optimization of the active area, width, and spacing of the electrode fingers [37–40]. Hence, they can be used for real-time, label-free, and in situ detection of target analytes [41]. However, the main drawback of these EIS-based sensors is their poor detection limit, compared to other electrochemical methods [5]. Contrastingly, a combination of electrochemical sensing techniques, for example, amperometry and impedimetry could enhance biosensor performance [42]. The details on different electrochemical detection methods are presented in Table 1.

When IDEAs are used in an amperometric redox amplifying biosensors, the interdigitated combs/fingers are called generator and collector electrodes. Redox cycling [43,44] occurs when redox species generated at the generator electrode (in an oxidation reaction) are collected at the collector electrode (in a reduction reaction) [45]. For this to occur, the generator and collector electrodes must be spaced close enough to overlap the diffusion layers of the redox species between the two electrodes [30,46]. A small gap between the finger electrodes allows for reversible redox species to undergo repeated oxidations/reductions (redox-cycling) before diffusing out to the bulk solution. The redox amplification factor is the ratio of the generator current in dual-mode operation (i.e., the generator and collector are at different enough potentials to allow for redox amplification) to the generator current in single mode (the generator and collector are at the same potential). The collection efficiency [47,48] is the ratio of the collector current to the generator current [49,50] or the ratio of the cathodic current to the anodic current at steady state [51]. The smaller the gap between adjacent comb electrodes, the shorter the diffusion time for the redox species to diffuse across the gap, resulting in a higher current amplification factor [46,49,52]. Due to redox amplification, IDEA-based electrochemical biosensors exhibit high signal-to-noise ratios, and thus better LODs, low ohmic drops, and rapid response time [53]. Furthermore, the efficiency of redox cycling and redox amplification factors can be further improved by increasing the height of the two working electrodes in a three-dimensional form [54]. The three-dimensional IDEAs (3D IDEAs) with their higher aspect ratio improve the contribution of linear diffusion between the electrode sidewalls and increase the IDEA's electrode surface overall area [49]. Another favorable microfabrication strategy, called the carbon microelectromechanical systems (C-MEMS) [55], offers the fabrication of high aspect ratio carbon IDEAs and is rendered simple and inexpensive through a one-step photolithography step of a polymer carbon precursor and subsequent pyrolysis [54,56].

The IDEA-based electrochemical biosensors provide easy-to-use and cost-effective fabrication, making them good candidates for portable point-of-care (POC) diagnostic devices [42,57]. This review focuses on the micro and nano size of IDEA-based electrochemical

biosensors, highlighting preferential fabrication techniques, including C-MEMS/NEMS technique, and their contributing factors to improve the sensitivity and selectivity of the electrochemical sensors by utilizing the amperometric and electrical impedance spectroscopy (EIS) detections for biomedical applications. This paper presents and discusses four-electrode configurations in electrochemical sensors using IDEAs as working electrodes in biomedical applications. Furthermore, a comparison between 2D IDEAs and 3D IDEAs was presented, focusing on the IDEA's width, gap, height modification, methods of increasing the 3D IDEA's surface area, and integration of nanoparticles to improve the sensitivity of the sensor performance.

Table 1. The working principle of electrochemical biosensors and their advantages and disadvantages.

Type of Electrochemical Biosensor	Working Principle	Advantages	Disadvantages	Refs.
Amperometric	Measures current resulting from redox cycling at a constant voltage (CA) and controlled potential (CV).	- Low fabrication cost; - High sensitivity.	- A signal reduction from fouling agents, and interferents in a sample.	[58,59]
Impedimetric	Measures impedance and changes in ionic concentration under no current flow between reference and ion-selective electrodes.	- Detect current changes without redox reaction; - Simple detection method.	- Slow dynamic response. - Low detection method;	[5,60]
Conductometric	Measures of conductance and interfacial electric arise from the biorecognition process.	- High signal-to-noise (S/N) ratio; - Directly detect the binding events; - No interference.	- Slow response; - Accuracy of detection depends on instrumental and experiment procedures.	[61]
Potentiometric	Measures potential difference from changes in ion concentration.	- No reference electrode; - Efficient at low amplitude alternating voltage; - Simplicity.	- Low specificity; - Low S/N ratio.	[62,63]

CV = cyclic voltammetry, CA = chronoamperometry.

2. Features in IDEA

2.1. Electrical Double Layer (EDL)

Figure 1 shows how the electrochemical IDEA-based sensor requires the interaction between target analyte/bioreceptor/electrolytic solutions and the sensor surface to produce an electrical signal. However, due to the various material sources for producing the electrode, such as carbon and metal, the interactions between the electrolytic solutions with the sensor create a phenomenon called electrical double layer (EDL) on the electrode surface [64–68]. The EDL is formed when the electrons in the electrode surface (e.g., metal) interact with ions in the electrolyte solution. Referring to the Gouy–Chapman–Stern (GCS) EDL model, the liquid solution creates two layers consisting of a compact layer and a diffuse layer [69]. The compact layer consists of the immobile solvent ions and molecules that adsorb into the solution/material interface, whereas the diffuse layer contains the mobile solution that carries solvated electroactive and inactive ions or the net charge within the liquid solution (Figure 2). The scattering of charges in the diffuse layer is determined by the Debye length, thus, providing the surface potential or charge of the material [70]. The EDL affected the electrochemical performance.

Yang et al. utilized computer simulation to study the effect of EDL in nanometer single electrode structure via the voltammetric performance. They reported that the extension of the diffuse layer into the diffusion layer in the EDL caused the increasing charge valence or the absence of the supporting electrolyte in the solution, which affected the current response of the nanometer electrode. It was reported that modifications to the thickness

of the EDL compact layer and its relative permittivity significantly influenced the current response [68,69,71]. Moreover, the ultramicroelectrodes, ranging from 25 µm to the sub-micrometer employed in published electrochemical experiments, were observed to cause nonlinear diffusion effects, resulting in enhanced mass transport, higher steady-state redox reaction rates, and faster response time, compared to larger electrodes [50,72–74].

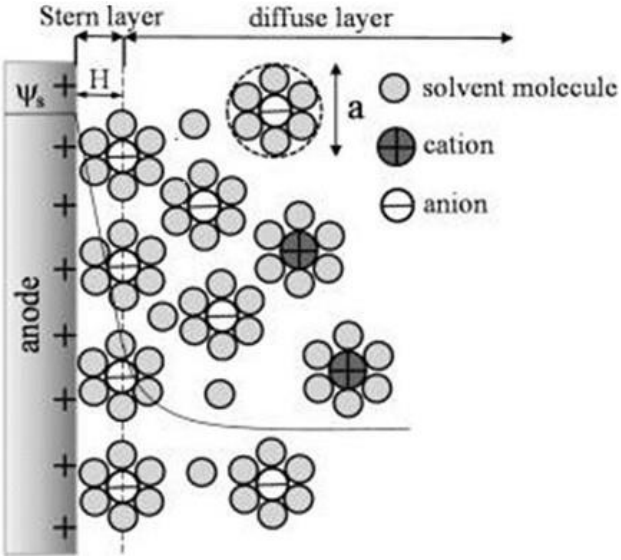

Figure 2. Schematic of the electric double layer structure showing the arrangement of solvated anions and cations near the electrode/electrolyte interface in the Stern layer and the diffuse layer of Gouy–Chapman–Stern model. Reprinted with permission from Ref. [75]. Copyright © 2022, American Chemical Society.

2.2. Crucial Parameters of the Sensor

Generally, the important parameters in performing biosensing are determined by sensitivity, selectivity, specificity, and limit of detection (LOD). In particular, the labelling method for target molecules is necessary for specificity, whereas the label-free method is more common for electrochemical detection using redox reaction [76]. The sensitivity of the electrochemical measurement method depends on the relations among the electron transfer between the molecule and the electrode, creating significant amounts of electrical current without any label.

In IDEA, the width and gap between adjacent fingers are crucial in the fabrication of IDEA-based electrochemical sensors. A smaller width will result in smaller capacitance, and hence faster mass transport of the species. In the pursuit to enhance the sensitivity of IDEA-based biosensors with lower detection limits, the design of IDEA itself offers practical manipulation in terms of increasing the number of widths within the array or lengthening the width. As a result, simple modifications may lead to higher faradaic current to capacitive current ratios and higher signal-to-noise ratios, producing highly sensitive biosensors suitable for biosensing applications. Furthermore, reducing the gap between adjacent fingers leads to a higher diffusional flux of redox species and enhances the rapid response at the collector, as well as sensor sensitivity [77].

Another factor to improve sensitivity of the biosensors for amperometric detection is redox cycling. Redox cycling between the narrow gap of the generator and collector of IDEA increase current response and signal-to-noise ratio [69,78]. A notable example was shown through work by Huang et al. [79] in which smaller gaps between electrodes, such as a 300 nm gap, were required for the dopamine detection of 2.89 nA/µM to achieve high feedback between the generator and collector electrode. The smaller gap size between adjacent fingers may enhance the current amplification due to the shorter diffusion time between the two electrodes' fingers [46,52,80].

Redox amplification also improves the selectivity of the biosensor, as it can selectively amplify reversible redox species of interest over irreversible species [30,49]. The specificity of the biosensor can be determined by the specificity of the biologically active materials and the target analytes. In this case, a probe incorporated with targeted biological components and a transducer convert the biochemical signals into electrochemical, acoustic, etc., [81]. In comparison, the optical method requires fluorescence detection or chemiluminescence with labels for biosensing detection. For example, green fluorescent protein (GFP) is a powerful tool to genetically encode a protein of interest (POI) for protein-based detection.

3. Micro and Nano IDEA

IDEA-based electrochemical sensors offer much potential in terms of the exploration of their functionality for practical biosensing applications. Considerable attention has been provided to unravelling the best substrates, electrode materials, and fabrication techniques and their influence on the IDEA's structures and geometries (e.g., width, the gap between adjacent fingers, and height), as well as sensitivity outcome [82–84]. Dizon et al. reported that the micron unit eased the analysis with a small sample size and helped to increase the sensor sensitivity for EIS measurement via the micron unit separation between working and counter electrodes [29]. Research found that IDEA is one of the versatile electrodes that allows the expansion of a three-electrode configuration (one working electrode) to a four-electrode configuration (two working electrodes) system. This is due to the advantages of the pair of comb fingers with the reference and counter electrodes available in the sensor setup. Moreover, miniaturized IDEA-based electrochemical sensors rose to fame, as reported in many recent studies, due to retainable electrode width, gap, and height in micro and nano units [85–87].

Interestingly, a preliminary study on the electric double layer (EDL), electric field distribution, and current density of IDEA can be performed numerically using finite element analysis (FEA) [88] software, such as COMSOL Multiphysics and ELECTRO. Finite element analysis simulation gives an early insight into the experimental outcomes and minimizes design errors [89–92]. The digital simulation helps researchers to predict the IDEA's electrical performance by virtually varying the height, gap, and width of IDEA [46,48,69,93–95]. The experimental results may differ from the simulation results as fabricated electrode dimensions and resultant EDL [69] may vary, affecting the overall sensor measurement [91,96]. Despite that, computational simulation offers early analysis of the sensor sensitivity from various electrode geometries and configurations, prior to actual fabrication.

3.1. Substrate, Electrode Material, and Fabrication Techniques

The substrates, electrode materials, and fabrication techniques are important criteria when fabricating IDEA-based electrochemical sensors. Most notable pieces of research employed carbon and metals as the source material of electrodes for IDEA by leveraging their advantageous properties, such as the semiconducting nature and excellent thermal and chemical properties that produce functional sensors with excellent sensitivity and selectivity.

3.1.1. Metal-Based IDEA

In addition to carbon-based IDEAs, metal/noble metals, such as Au, Pt, Al, Fe, and organic/inorganic-based nanoparticles, have been used as IDEA's electrode materials, with gold (Au) [91] or platinum (Pt) being the most popular selections for IDEA's starting materials [97]. Gold has many favorable properties, such as inertness, biocompatibility, resistance to oxidation, high conductivity, compatibility with surface functionalization methods, and suitability to being manufactured in ranges of nanosizes [98,99]. The advantages of gold have been employed in the development of highly sensitive, selective, and stable analytical devices in many biosensing applications [100,101]. Thus, several reports on

IDEA-based metallic sources are presented for comparison in terms of fabrication methods and sensor achievements.

The important types of substrates and fabrication techniques have been highlighted and compared. Rishi et al. studied three types of IDEA fabrication techniques and substrates (copper-cladded IDEA, laser-induced graphene IDEA from polyimide sheet (LIG-based IDEA), and 3D-printed graphene filament IDEA) with constant width = 917 µm, gap = 553 µm, and all three IDEA sensors tested for *Escherichia coli* (*E. coli*)-sensing using impedimetric sensing [102]. In this research, they found that the LIG-based IDEA presented the best sensitivity, with detection (LOD) as low as 2.5 CFU/mL, tested using *E. coli*, and the best selectivity by producing the least amount of interference in the presence of 1.008×10^5 CFU/mL *E. coli* and Shewanella Oneidensis bacteria concentration, respectively. Moreover, the LIG technique was reported to have a relatively short fabrication time with the cheapest costs, compared to the other two techniques.

Another commonly used material to fabricate IDEA is platinum (Pt). For instance, Matylitskaya et al. [18] fabricated Pt nanogap IDEAs (nIDEAs) on silicon (Si) substrate for Lab-on-a-Chip applications (LoC). Ferrocenemethanol (FcMeOH) and p-aminophenol (pAP) were used as the redox couples to perform CV and CA electrochemical characterization of Pt nIDEAs. The Pt nIDEAs (g = w = h = 100 nm) obtained an amplification factor of 161 with 1 mM FcMeOH and an amplification factor of 118 with 1 mM pAP, respectively, with collection efficiency of more than 99% for both tested FcMeOH and pAP. Thus, Pt can be considered as one of the promising metallic materials in fabricating IDEA-based biosensors with enhanced performance and sensitivity [103,104].

Taking advantage of gold (Au) as IDEA's electrode material, a combination of two Au-IDEAs in supercapacitors has been studied by Ferreira et al. [105]. They created a supercapacitor using an electropolymerization method to graft the polypyrrole/carbon nanotube (PPy/CNT) nanohybrid film on two Au-IDEAs (∼60 nm thickness, 10 µm width, and 10 µm gap) followed by investigation on electrochemical analysis, impedimetric sensing, and PPy/CNT nanocomposite synthesis. They immobilized Anti-Cystatin C (Anti-CysC) on IDEA via ethylenediamine bifunctional agent, glycine blocking in acid, and alkaline medium using covalent entrapment. Based on their result, the IDEA immunosensor to CysC capacitive effect of the antigen–antibody interaction serum was detected by double-layer capacitance under low frequency and the response was measured by changes on the phase angle with a linear range of up to 300 ng/mL. They also calculated the cut-off point for the serum sample and their results showed a total reduction in non-specific binding at approximately 28 ng/mL CysC. To maximally minimize non-specific binding, the blocking agent of glycine was used in two different mediums (alkaline and acid) for the IDEA immunosensor [105]. Oh et al. studied the label-free electrochemical immunosensor using gold IDEA (Au-IDEA) modified with self-assembled monolayers (SAMs) and IL-6 antibodies (IL-6 mAb) for the prompt detection of traumatic brain injury (TBI) by quantifying cytokine interleukin-6 (IL-6) in cerebrospinal fluid (CSF) [106]. Their sensor was tested using EIS and showcased excellent selectivity and LOD of 1.63 pg/mL.

3.1.2. Carbon-Based IDEA

Highlighting the advantages of carbon as an electrode material, C-MEMS/C-NEMS is one of the emerging fabrication techniques in fabricating carbon-based IDEAs, due to the simplicity of the fabrication steps and the ability to produce a high aspect ratio IDEA. The carbon microelectromechanical systems (C-MEMS) and carbon nanoelectromechanical systems (C-NEMS) fabrication techniques allow the production of high aspect ratio of carbon structures via a conventional photolithography technique to pattern the desired shapes of photoresist polymers followed by pyrolysis [107]. As a result, electrodes with carbonized patterns can be easily fabricated according to desired structures and geometries. An epoxy-based photoresist, SU-8, is a good substance to fabricate high aspect ratio structures. SU-8 is a highly sensitive negative tone photoresist that exists in various viscosities, influencing the resultant thickness of patterned surfaces, ranging from hundreds of micrometers to

submicron levels [108]. Due to the flexibility of the deposition thickness, SU-8 is one of the popular substances used to fabricate high aspect ratio structures using lithography methods. The lithography methods can be categorized into two types, namely masked lithography and maskless lithography. As reflected by the name, masked lithography method is used to transfer a pattern onto the substrate using a mask. Ultraviolet (UV) photolithography is one of the masked lithography methods [109,110]. Photolithography is a patterning method that uses UV light exposure to light-sensitive polymers (photoresist) to create the desired patterns. The illumination of UV light via an opaque feature of a photomask positioned on a transparent substrate creates an exposure on a photoresist, which is coated on a substrate [55,111,112]. Wang et al. pioneered the high aspect ratio C-MEMS devices with the ratio of 10:1 [113]. In later years, following the first report, many research works adapted a similar strategy to fabricate their C-MEMS and C-NEMS devices [114–116].

Figure 3 showcases the difference between the 2D and 3D designs of the C-MEMS electrode. The fabrication of 2D and 3D C-MEMS requires the photopatterning of the base layer (e.g., the IDEA) with a thickness ranging from 5–25 μm for 2D, while 3D requires the patterning of the second layer on top of the first layer. However, the second layer of the 3D pattern can be manipulated using the mask design. Then, the pattern is pyrolyzed under an inert atmosphere at temperatures above 600 °C to produce carbon structures. Pramanick et al. reported that the optimized temperature for electrochemical sensing applications is 900 °C [83]. In addition to the simplicity and fewer fabrication steps, the advantages of the fabrication techniques of C-MEMS and C-NEMS include low cost, good control of resistivity, and mechanical properties of carbon by varying the temperature of pyrolysis, controlling the porosity by varying the temperature ramp rates, and having high reproducibility [117].

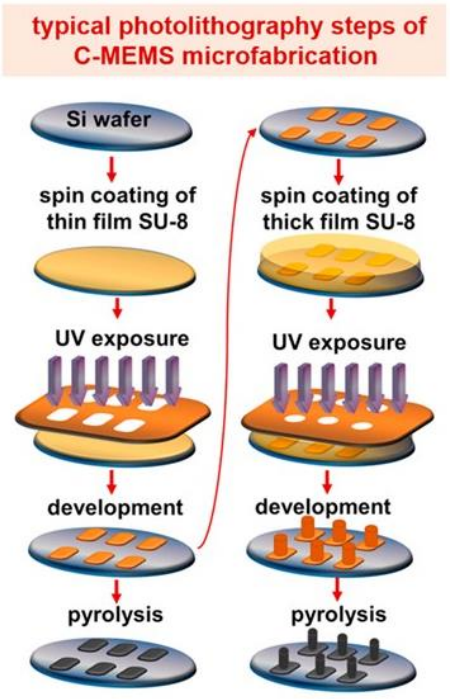

Figure 3. Schematic illustration of a typical photolithography process to fabricate 2D and 3D C-MEMS electrodes. Reprinted with permission from Ref. [118]. Copyright © 2022 Elsevier B.V. All rights reserved.

As such, Liu et al. [119] compared the expected simulation response with the IDEA fabricated via C-MEMS technique. They compared five different IDEA gaps (g) between

2.7 μm and 16.7 μm, and widths (w) between 1.3 μm and 2.3 μm. They reported that the smallest electrode gap spacing of 2.7 μm and an electrode width of 1.3 μm recorded the highest steady-state currents in the generator/collector mode 4.7 μA (experimental) and 3.8 μA (simulation) at a scan rate of 10 mV/s, as well as a collection efficiency up to 98%, revealing that approximately all products from the generator have reached the collector. For larger IDEA gaps, they obtained quantitative agreement between simulation and experimental data, but for the smallest IDEA electrodes, they recorded larger currents than the predicted simulation. The authors concluded that this could be due to convection caused by electrokinetic flow.

The combination of metal and carbon in IDEA have proved enhancement of the collection efficiency of IDEA-based electrochemical sensors. A follow-up study by Liu et al. [120] compared the CV performance of the carbon–platinum IDEA (C-Pt IDEA) with a carbon–carbon IDEA (C-C IDEA) [119], using homogeneous catalytic production of hydrogen (H_2) as the test redox system [120]. The width of the carbon generator electrode was 2 μm (slightly wider because of overplating of the Pt), and the gap between two adjacent fingers was 3 μm. They found that in the same H_2 production reaction, the C-Pt IDEA current was higher (collection efficiency 68%) than the C-C IDEA (collection efficiency 37%) in the presence of acid. However, they also observed that the combination of the C-Pt IDEA did not achieve higher collection efficiency in the presence of acid. Thus, their findings proved that the addition of Pt on C increased collection efficiency for the homogeneous catalytic production of hydrogen (H_2).

3.2. Method to Increase Surface Area in IDEA-Based Electrochemical Sensor

In an effort to maintain the IDEA electrode measurement within nano to micro sizes, the sensitivity and specificity of 3D IDEA-based electrochemical sensors can be facilely controlled via manipulation of the IDEA geometries and structure, integration of microchannels, integration of nanoparticles, and fabrication of IDEA from various substances as electrode materials. Escalations in the height of 3D IDEA increase surface area and diffusion area in electrolytic solutions. As a result, redox amplification in electrodes increases and improves the sensor sensitivity. Furthermore, the sensitivity of the electrochemical sensor from IDEA is label-free and highly functional for practical biosensing applications. The selectivity can be determined by the labelling method between the target analyte and receptor in some cases.

3.2.1. Microchannel Insertion

The electrochemical responses of the electrode with the integration of the microchannel are affected by several factors, such as solution flow rate, dimensions of the electrode and the channel, the potential sweep rate, etc. [121]. The miniaturization of the IDEA's electrode dimension with channel encapsulation does improve the redox reaction but changes the radial diffusion on the IDEA. Additionally, Heo et al. [49] studied the simulation of 1:1 aspect ratio of two types of 3D IDEA nanoelectrodes that have similar width (w = 650 nm) and electrode gaps (g = 2.35 μm) but different heights (3D IDEA nanoelectrode (h = 650 nm)). They further investigated the electrode ratio effect on redox cycling and the influence of different microchannel heights (h = 1 to 10 μm) on a 3D IDEA thin-band nanoelectrode (h = 100 nm). Their team reported that the lowest height of the microchannel interrupted the radial diffusion to the electrodes and caused the decrease in diffusion to the top surface, thus, reducing the total current. Moreover, their simulated sample confinement also enhanced the collection efficiency up to 98%, which aligned with Ueno et al. [121,122] who reported that collection efficiency in the presence of a microchannel was higher than without a microchannel.

The integration of the microchannel affected the electrochemical sensor performance and increased the IDEAs' whole surface area too. As such, Heo et al. [49] fabricated carbon 3D IDEA nanoelectrodes from SU-8 negative photoresists using the C-MEMS method integrated into the polydimethylsiloxane (PDMS) microchannel for dopamine applica-

tion. Interestingly, they found that chronoamperometry (CA) recorded the highest signal amplification at 1116 with a 10 μm high microchannel, when performed for the same duration as both single-mode and dual-mode currents. It was concluded that channel height caused higher dual-mode currents (3.38 mA), compared to single-mode current (3.03 nA), due to the sample confinement affected by the reduction in single-mode current. They also measured various concentrations (10 μM to 10 mM) of dopamine in 0.1 mol L^{-1} phosphate-buffered solution (PBS) to test the carbon biosensor applicability. The adsorption of dopamine caused large iR drops and lost linearity in the electrochemical current response when the biosensor was tested in high-dopamine solutions. Nevertheless, in low concentrations, the redox currents became well saturated, which means the carbon 3D IDEA nanoelectrodes surface was less vulnerable, compared to metal electrodes when the chemical reaction of dopamine occurred. Thus, the integration of the microchannel affected the electrochemical sensor performance and increases the IDEA's whole surface area.

The study of flow and no flow conditions in microchannel does perturb the sensor sensitivity. Kamath et al. [54] presented the 3D carbon microelectrodes IDEA from low-viscosity negative photoresists (SU-8 2000.5, SU-8 2002, and SU-8 2005) material, fabricated using C-MEMS. They analyzed the sensor performance under flow and no-flow conditions using CV and CA. The 3D IDEA was enclosed in a PDMS channel (100 μm high and 1.5 mm wide), as shown in Figure 4, to ensure little evaporation of the solution during the experiment. Their study showed that an increase in 3D carbon IDEA height (height of 1.1 μm) and a width/gap ratio of 1.58 (w bottom = 2.7 μm, w top = 1.95 μm, gap bottom = 1.1 μm, and gap top = 1.85 μm), which increases the redox amplification factor to 37 with a collection efficiency of 98.6%. Their results showed that amplification dropped from 37 to 4 for the same IDEA electrode at a flow rate of 500 nL/s due to redox cycling hindered by the convection. Under no-flow conditions, an increase in the IDEA's height caused higher redox amplification, whereas, under flow conditions, lower signal enhancement was being detected because the flow was detrimental to the elliptical diffusion between the horizontal edges of the 3D carbon IDEA. Their team focused on higher and wider IDEA's height and width in μm unit, while their gap spacing used was smaller than Heo et al. [49], which proved the advantages of the smaller gap spacing in carbon IDEA's design. However, further details on the flow and no-flow conditions in PDMS microchannel with the different heights of a microchannel affecting the redox amplification was not studied. The lower height of the microchannel (less than 100 μm) should be considered and incorporated for further studies of flow and no-flow conditions and their consequences on IDEAs' sensor performance.

3.2.2. IDEA Geometry and Structures

The IDEA-based sensors have been extensively explored [123–125]. Several works have demonstrated that higher IDEA thickness or height of the electrodes results in higher redox amplification factors [49,54,126,127]. In addition, increasing the surface area of IDEA-based sensors can be achieved in various ways, such as by fabricating pillars on top of the 2D IDEAs [128,129], by controlling the spin-coated thickness and shape of the photoresist carbon precursor material [54,130–134], and by growing vertically aligned carbon nanotubes (VACNT) on top of planar IDEA [135,136]. Interestingly, without increasing the extent of the IDEA's thickness, the integrated microchannel [121,137,138] and combination with a mesh [139] on IDEAs does improve the amplification factor due to the large surface area of the redox cycling event. In addition, the design of 3D IDEA sensors will also improve the sensitivity [140] and redox amplification/amplification factor, compared to planar IDEA sensors.

Current research has shown that simulation and comparison of the 2D IDEA and 3D IDEA are indeed important to provide empirical results prior to the actual fabrication of 3D IDEA biosensors for targeted biosensing applications. The comparison between the simulation and actual experiment of 2D IDEA and 3D IDEA was published by Han et al. [141]. They studied four different systems of the geometric configuration effect of IDEA electrodes, which are Open-2D IDEA, Closed-2D IDEA, two straight electrodes in parallel,

and 3D IDEA using the simulation process from COMSOL Multiphysics software. From these four patterns of geometric configuration, 3D IDEA simulation has the best result for electrochemical immunosensing. Subsequently, they fabricated the 3D IDEA using photoresist AZ4620 with modification to the indium tin oxide (ITO) electrode, alkaline phosphatase (ALP) as the enzyme label, electroactive ferrocene (Fc) as the electron mediator, and p-aminophenyl phosphate (pAPP) as the enzyme substrate. They demonstrated that 3D IDEAs consisted of a thin layer of solution narrowed between the two IDEA electrodes with a 5 µm width and 10 µm gap between the bottom and the ceiling height (several tens of µm), corresponding to the height of the microchannel. They also tested their biosensor using amperometric and chronocoulometric methods besides impedimetric detection. Their proposed fabrication technique also required no addition of biological additives. They tested the 3D IDEA immunosensor for mouse IgG and cardiac troponin I (cTnI). Based on their results, the 3D IDEA achieved an LOD of ∼10 fg/mL and ∼100 fg/mL for the Closed-2D IDA for detection limit in mouse IgG, whereas 3D IDEA obtained a limit of detection of 100 fg/mL for cTnI. Their findings proved that 3D IDEA did not only increase the surface area but also decreased the LOD values.

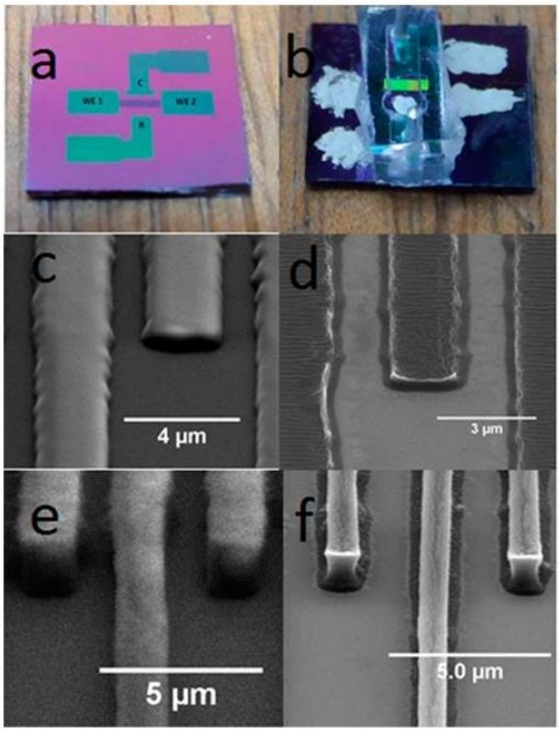

Figure 4. (**a**) 3D carbon IDEA sensor on a Si wafer. WE1 and WE2 are contact pads for the generator and the collector, respectively. C and R are counter and reference electrodes, respectively. (**b**) 3D carbon IDEA integrated with PDMS channels. The reference electrode is coated with Ag/AgCl ink, and contact pads are coated with silver paste for better electrical connection. (**c**,**e**) Scanning electron microscopy (SEM) images (tilted view 60°) under 10,000 × magnification of SU-8 IDEA patterning before pyrolysis; height = 0.6 and 2.1 µm, respectively. (**d**,**f**) Carbon IDEA after pyrolysis; height = 0.22 and 0.59 µm, respectively. Reprinted with permission from [54]. Copyright © 2022, American Chemical Society.

Moreover, shrinkage is one of the factors that changed the height during the pyrolysis step. In addition to the height or thickness of spin-coated materials building up into one solid rectangle shape for the whole width of the IDEAs' finger array during the photolithography technique, the modification of IDEA geometry into a pillar-shaped array and onto the IDEA's fingers transforms the whole shape of the basic 3D IDEA pattern. This has been reported by Amato et al. [129]. Their team demonstrated a high aspect ratio of

3D carbon pillars synthesized from SU-8 2075 on top of SU-8 2005-based planar 2D carbon IDEAs. Figure 5 illustrated the C-MEMS fabrication process using the negative photoresist materials followed by analysis via CV and EIS for further investigation of their sensor performance. They successfully fabricated 3D carbon pillars with 1.4 μm diameter, a centre-to-centre spacing of 5 μm, and an aspect ratio of about 8 and 11 μm in height. Their team also described the shrinkage of planar 2D IDEAs that interconnects the pillars yield carbon digits (a decrease of 91.7 ± 0.5% vertically) and width (a decrease of 27 ± 3% laterally) from what was originally 5 μm width and thickness. The 3D carbon pillars shrunk to 1.4 μm in diameter and 11 μm in height. The pyrolysis process resulted in a loss of material caused by the evaporation of CO_2, hydrocarbons, and other gases during photoresist decomposition and aromatization, leading to the shrinkage of the structure [142]. Their team achieved a high aspect ratio 3D IDEA that produced a quasi-reversible CV with a peak potential separation (ΔEp) value of 168 ± 12 mV. Their presented 3D IDEA's pillar array successfully increased the surface area up to 70%, compared to the same electrode without pillars.

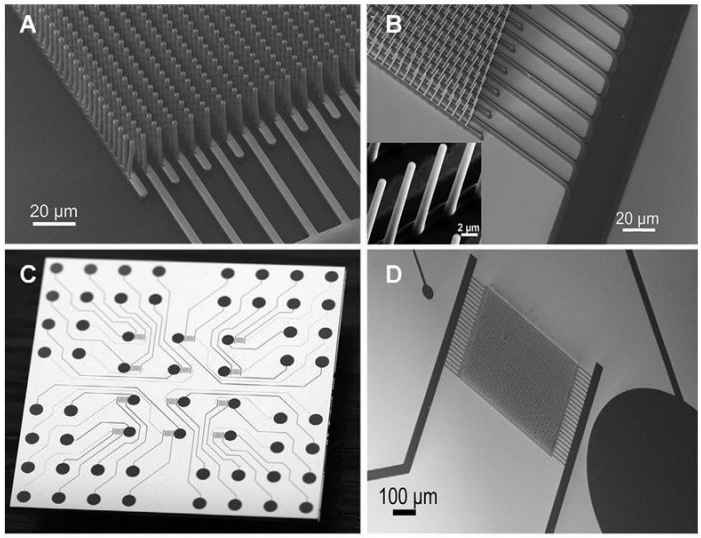

Figure 5. SEM images of 3D IDEAs with carbon pillars (diameter of 1.4 μm, height of 11 μm) interconnected by interdigitated structures: (**A**) before pyrolysis; and (**B**) after pyrolysis. (**C**) Photograph of a silicon chip with the pyrolyzed carbon electrode array structures (12 three-electrode systems at the center with surrounding contact pads). (**D**) SEM image of a three-electrode system. Reprinted from [129], Copyright © 2022 Elsevier Ltd. All rights reserved.

Another type of 3D carbon pillar was mentioned by Bose et al. [143], whereby their team fabricated a 3D carbon IDEA in which their 3D pillar expressed a shape that was similar to that of Amato et al. [129]. In contrast, the diameter of their pillar was 20 μm on top of the 2D IDEA. They spin-coated the SU-8 2000 on quartz as the substrate, followed by infrared lithography and pyrolysis. Their conductive carbon-based capacitive IDEA sensor exhibited a sensitivity value of 2.741 μA mM^{-1} cm^2 for glucose testing. The difference was that they used quartz as a substrate instead of silicon. Therefore, these finding highlighted the importance of a substrate in the fabrication of functional electrodes [144].

The aforementioned carbon 3D IDEA design showed a clear boundary between collector and generator fingers with enhanced surface area. The challenging elements of increasing the surface area of carbon 2D IDEA to 3D IDEA have been explored by adding the suspended beam on top of the existing pillars forming a unique 3D IDEA architecture (see Figure 6). Interestingly, Mantis et al. [145] fabricated a complex IDEA from the carbon-based 2D IDEA to the novel suspended carbon 3D IDEA using three types of photoresists via C-MEMS technique and tested their electrodes using CV and EIS. Their team fabricated 3D interdigitated electrodes with pillars on different fingers connected through suspended interdigitated microstructures, as shown in Figure 6a,b. The bottom

part composed of 2D IDEA was synthesized from SU-8 2035. The micropillars were fabricated from SU-8 2075, whereas the suspended layers consisted of mr-DWL-40 photoresist. Their team successfully increased the 3D IDEA surface area by adding the suspended IDEA supported with micropillars onto the 2D IDEA pattern. Both the fingers of interdigitated electrodes were used as an electrode in which one of the interdigitated carbon electrodes suspended carbon IDEA dimensions; $2D_p$-25, $3D_{\#}$-25 bottom IDEA and pillars: w_{bot} = 25 µm, s_{bot} = 25 µm, t_{bot} = 17 µm, d = 20 µm, s_{pil} = 60 µm, h_{pil} = 100 µm, and $3D_{\#}$-25 suspended IDEA: w_{sus} = 10 µm, s_{sus} = 20 µm, t_{sus} = 17 µm. The highest anodic steady-state current, $I_p = 0.527 \pm 0.003$ mA, was achieved by $3D_{\#}$-25, while for 2D IDEA, the $2D_p$-25 recorded highest $I_p = 0.23 \pm 0.02$ mA. Their results proved that $3D_{\#}$-25 increased the surface area of the electrode as it recorded a three times larger CV peak current, compared to the 2D electrode, $2D_p$-25. Their findings emphasized that the complex was used as WE and the other one as CE for both CV and EIS. The 3D-suspended carbon 3D IDEA was a method used to increase the IDEA's surface area, improving the sensor performance, compared to the original carbon 2D IDEA.

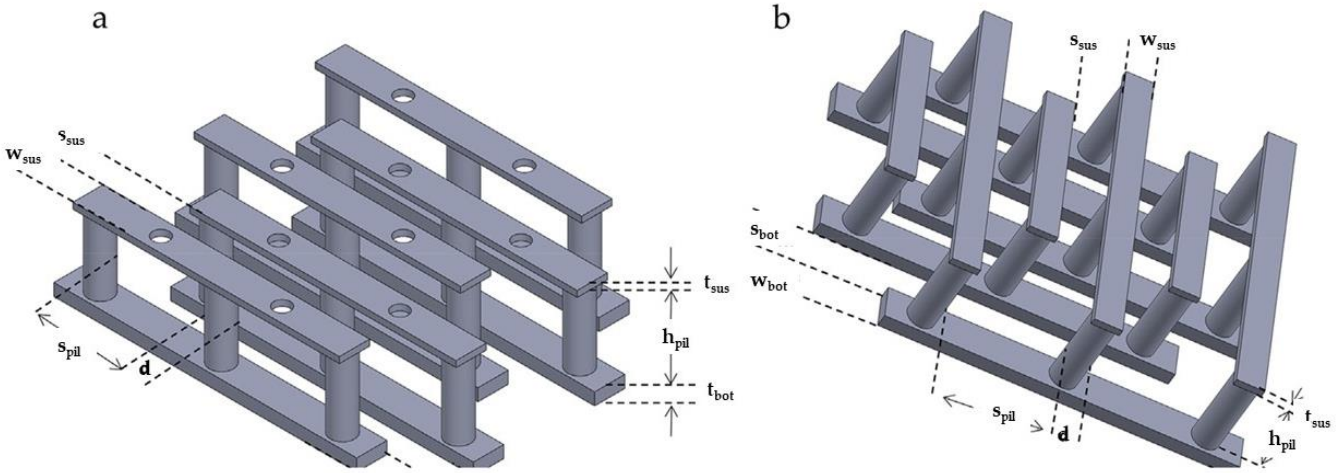

Figure 6. Suspended layer with: (**a**) stripes connecting pillars of the same finger (3D//); and (**b**) stripes connecting different fingers of the same electrode ($3D_{\#}$). Reproduced from [145]. Copyright © 2022, Elsevier under the terms of the Creative Common CC-BY license.

Another interesting piece of research to increase IDEA sensor performance while retaining the IDEA original structural layer was conducted by Sharma et al. [139] in which they added the mesh-like shape on top of a carbon 3D IDEA. Continuing the IDEA fabrication process using C-MEMS, they produced a 2 µm thick SU-8 2002 positive photoresist (AZ P4330) coated on top of a pre-patterned carbon IDEA, followed by the spin coating of 18 µm thick SU-8 2025. The unique IDEA fabrication method of using a small UV dose through a mesh-shaped photomask successfully facilitated the shallow polymerization of the top layer of spin-coated photoresist. A 5 µm thick suspended polymer mesh supported by two 18 µm thick posts was achieved after the development of a double exposed negative photoresist followed by pyrolysis. The substrate-bound IDEA gap of ~1.9 µm and a few micrometers apart from the suspended carbon mesh (width ~300 nm) are shown in Figure 7. The CV dual-mode resulted in high signal amplification of ~25 from redox cycling of PAP/PQI, compared to single-mode CV. Their 3D carbon immunosensor recorded a linear detection range of 0.001 to 100 ng/mL for cardiac myoglobin (cMyo). The immunosensor successfully recorded a low detection limit of 0.43 pg/mL cMyo in phosphate-buffered saline and human serum [139]. Their distinctive method for improving the IDEA-based sensor proved that the C-MEMS technique is not only limited to the simple fabrication of 3D IDEA design but is also capable of producing a distinct mesh shape.

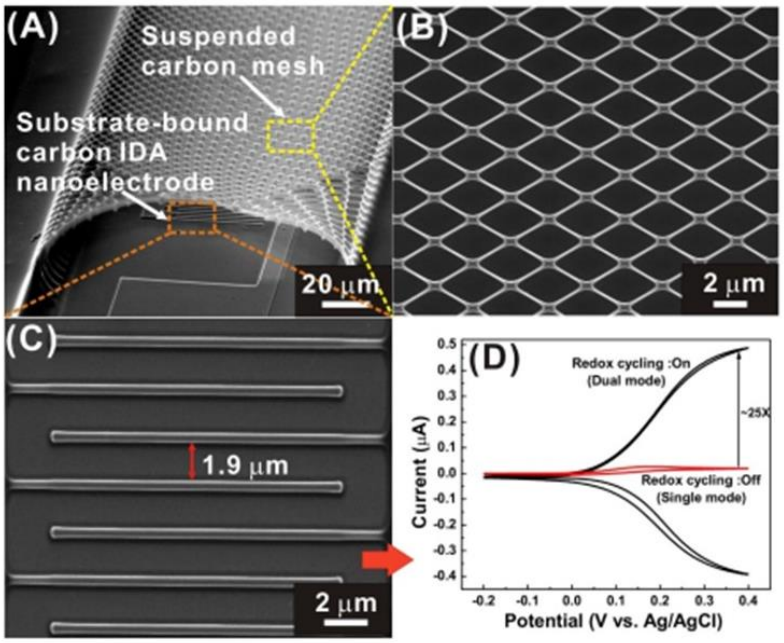

Figure 7. (**A**) SEM image of a 3D carbon system (tilted-view); (**B**) enlarged top-view images of a suspended carbon mesh; (**C**) substrate-bound carbon IDEA nanoelectrodes; and (**D**) cyclic voltammograms of 1 mM PAP in 0.1 M PBS at the IDEA nanoelectrodes. Both the combs were scanned from −0.2 to 0.4 V vs. Ag/AgCl in the single-mode (red line). In the dual mode, the potential of the generator comb was scanned the same as the single-mode while the collector comb was held at −0.3 V (black line). Amplification factor (AF) = sum of dual-mode current from IDEA/sum of single-mode current from IDEA. Reprinted from [139]. Copyright © 2022 Elsevier B.V. All rights reserved.

3.2.3. Three-Dimensional (3D) IDEA in a Two-Electrode Configuration

Generally, IDEA's four-electrode configuration requires a reference electrode and a counter electrode. Interestingly, Lee et al. [146] eliminated the reference electrode and counter electrode in their IDEA-based electrochemical sensor, leaving the IDEA integrated into the microchannel to increase the surface area. The research team fabricated the 3D IDEA using a similar method as that published by Han et al. [141] albeit with modifications. They modified the four-electrode (4E) system (consisting of two working electrodes, the counter and reference electrode) to a two-electrode (2E) system, alternatively aligned with a 5 μm wide, 10 μm gap between adjacent fingers, and a height that depended on the height of the channel (30 μm) without the counter and reference electrode, as shown in Figure 8 [146]. They successfully established their IDEA working principle by introducing a redox mediator film, poly(methylene green) (PMG), immobilized with poly(dopamine) (PDA) onto the indium tin oxide (ITO) 3D IDEA chip configuration by electropolymerization. Uniquely, one of the working electrodes was used to observe the electrochemical signal, whereas the other working electrode worked simultaneously as counter and reference electrodes in which oxidation and reduction occurred. This is an interesting piece of work, compared to the previous carbon 2D IDEA and 3D IDEA. In this research, they further tested the 2E system of ITO 3D IDEA with human creatine kinase-MB (CK-MB) and a detection limit of 0.32 pg/mL was achieved, confirming the fabrication of reliable and highly sensitive electrodes. The advantage of their two-electrode IDEAs system was that any electrodes can be fabricated from the same starting materials, resulting in a less complicated fabrication process. In future, their distinctive IDEA testing without reference and counter electrodes can be further explored and may be applied for carbon IDEA with some modifications to the carbon surface. In addition, Table 2 summarized the comparison between the carbon-based 2D IDEA (2D C-IDEA) and carbon-based 3D IDEA (3D C-IDEA) sensor performance using CV based on amperometric sensing technique.

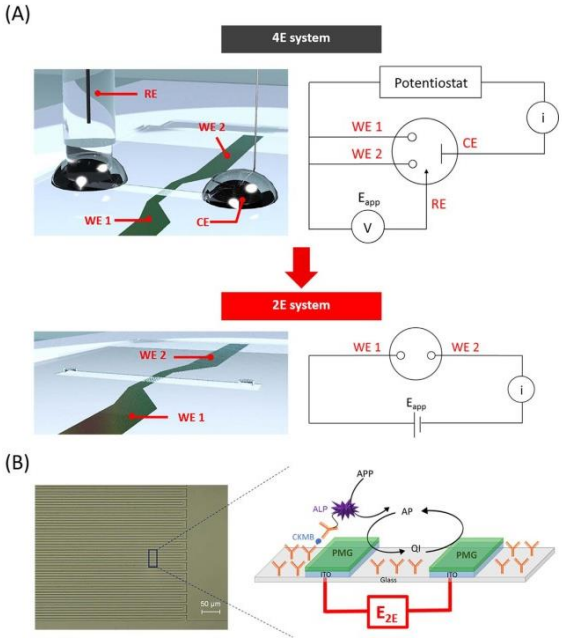

Figure 8. (**A**) Scheme of four-electrode (4E) and two-electrode (2E) systems in IDEA microchip; (**B**) optical microscopic image of IDEA and schematic representation of electrochemical immunoassay in IDEA microchip. Illustrations of cross-sectional view of IDEA surface showing immobilization of antibodies onto a glass substrate, where ITO is etched, followed by immobilization of PMG with dopamine (DA) onto ITO. Reprinted from Ref. [146]. Copyright © 2022 Elsevier B.V.

Table 2. Comparison between carbon-based 2D IDEA (2D C-IDEA) and carbon-based 3D IDEA (3D C-IDEA) sensor performance using CV based on amperometric technique.

Electrode C-IDEA Sources	Dimension	IDEA Structure	Sensor Performance	Ref.
SU-8	w = 650 nm, h = 650 nm, g = 2.35 µm	3D C-IDEA	(1) AF = 10.8, CE = 96.8% in bulk solution (2) AF = 139 in h = 6 mm channel, (3) AF = 230 in h = 10 mm channel	[49]
SU-8 2000.5, SU- 8 2002, SU-8 2005	h = 1.1 µm and a w/g ratio of 1.58 (w bottom = 2.7, w top = 1.95, g bottom = 1.1 µm and g top = 1.85 µm)	3D C-IDEA	AF = 37, CE = 98.6%	[54]
SU-8	w = 1.3 µm g = 2.7 µm	2D C-IDEA	AF = 13, CE = 98%	[119]
SU-8, Pt	w < 2 µm, g < 3 µm	2D C-Pt IDEA	CE = 68%, 31% higher than C-C IDEA	[120]
SU-8 2005, SU-8 2075	(1) g = 5 µm, (2) 2D C-IDEA: h = 0.4 µm, w = 3.6 µm (3) 3D C-IDEA: h = 11 µm, diameter = 1.4 µm	3D carbon pillars on top of 2D C-IDEA	CV: 168 ± 12 mV for carbon 3D IDEA with pillars of 1.4 µm in diameter (aspect ratio of 8)	[129]
SU-8 2035, SU-8 2075	2Dp-25 and 3D#-25 bottom IDEA and pillars: w_{bot} = 25 µm, s_{bot} 25 µm, t_{bot} = 17 µm, d = 20 µm, s_{pil} = 60 µm, h_{pil} = 100 µm, 3D#-25 suspended IDEA: w_{sus} = 10 µm, s_{sus} = 20 µm, t_{sus} = 17 µm	2D C-IDEA and 3D C-IDEA with suspended	3D#-25: I_p = 0.527 ± 0.003 mA, $2D_p$ − 25: I_p = 0.23 ± 0.02 mA	[145]

AF = amplification factor, CE = collection efficiency.

4. Nanocomposites IDEA

4.1. Vertically Aligned Carbon Nanotube (VACNT)

In addition to the modification of carbon 3D IDEA's height structures, another method for increasing the IDEA's surface area and sensor sensitivity is through the integration of porous vertically aligned carbon nanotubes (VACNT) onto the IDEA design. Brownlee et al. [136] investigated the IDEA design surface area by fabricating a porous 3D VACNT IDEA and comparing it with a serpentine electrode using CV and EIS, as shown in Figure 9. They fabricated four electrodes of 3D VACNT IDEA and two serpentine (SE) electrodes where the width and gap for 3D VACNT IDEA and SE were similar; the width of the electrode (w = 20 µm and 25 µm), the gap between adjacent fingers (gap width, g = 15 µm and 25 µm), and height for 3D VACNT IDEA (h = 5 µm, 25 µm, and 80 µm) and SE (h = 80 µm). Their fabrication method did not employ the C-MEMS method; instead photolithography was used to pattern the positive photoresist AZ3330 with Fe as the substrate. The growth of VACNT followed published protocols [147,148]. Based on CV and EIS analyses, they found that the 3D VACNT IDEA (h = 80 µm and g = 15 µm) resulted in 1.6 times higher sensitivity than SEs and had 4.3 times higher sensitivity, compared to the 5 µm height 3D VACNT IDEA. The biosensors were then tested with streptavidin and biotin. The 80 µm height of the 3D VACNT IDEA with a gap of 15 µm demonstrated an LOD of 1 ng/mL F-biotin, equivalent to other reported work [149,150]. It has been found that the promising electrodes expressed the highest sensitivity, most linear-sensing regions, and an electroactive surface area of 15 times higher than the 2D geometric area. These findings showed that the integration of VACNT on metal IDEA structure can potentially enhance the biosensor's sensitivity.

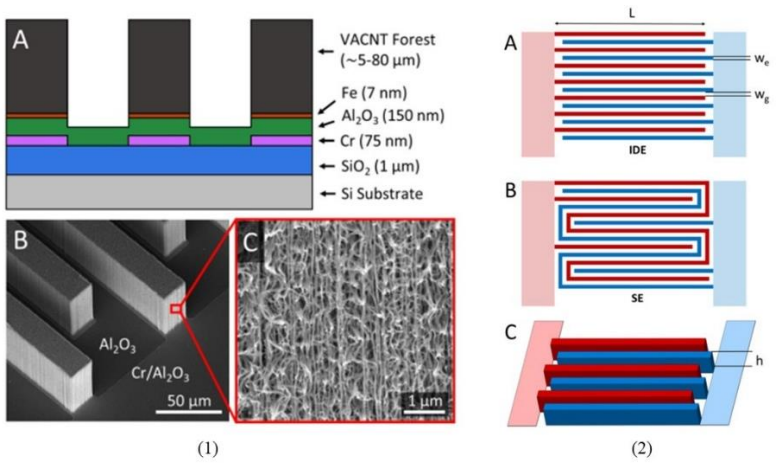

Figure 9. (1) (**A**) Schematic of layers used to fabricate the VACNT sensor architecture: Si, SiO_2, Cr, Al_2O_3, Fe, and VACNTs; (**B**) scanning electron microscopy (SEM) images of 3D VACNT electrodes; and (**C**) magnified VACNTs, showing the porous nature of an electrode. (2) Schematic of the: (**A**) IDE; and (**B**) SE electrode arrangements with electrode length (L), electrode width (we), and gap width (wg) represented. Red and blue distinguish the different electrodes in the sensor, with the dark colors representing regions of VACNTs and light colors representing Cr leads under Al_2O_3. (**C**) Schematic emphasizing the 3D nature of VACNT IDEA electrodes with electrode height (h) represented. Reprinted with permission from [136]. Copyright © 2022, American Chemical Society.

In a similar piece of work, Ding et al. [151] used silicon/silicon oxide wafer, AZ3330 resist, and iron catalytic layer as the IDEA base to fabricate 3D VACNT IDEA (labeled as VANTAs). However, the modification performed by Ding and colleagues focused on the height-to-width ratio of 3:1, whereas Brownlee et al. [136] compared 3D VACNT IDEA (different w, g, and h dimensions) with the serpentine electrodes. They reported a 2D IDEA pattern for their immunosensor CIP2A using non-carbon electrode material followed by testing using CV. In situ amorphous carbon infiltration into the CNT forest was performed to produce robust and porous arrays of IDEA fingers. These immunosensor exhibited the

detection of label-free CIP2A across a wide linear-sensing range (1–100 pg/mL) with an LOD of 0.24 pg/mL within saliva supernatant without the need for sample pre-labelling or pre-concentration methods. Moreover, the faradaic EIS detection method used for these immunosensors did not require a three-electrode electrochemical setup or reference electrode to make the VACNT IDEA fit for mass fabrication, miniaturization, and integration into microfluidic channels [151,152]. They also reported that the approximate 1% of active sites at a scan rate of 50 mV/s in CV was greater than the approximate 0.4% of active sites from previous reports [153]. Hence, the porous architecture of VACNT IDEAs is advantageous in elevating the electroactive surface area beyond a conventional solid or planar IDEA sensor [154], and it also offers better active sites or carbon–carbon defects, compared to conventional CNT electrodes [151,155,156].

4.2. Nanoparticles

Nanoparticles are particles ranging between 1 and 100 nm and are typically categorized into organic, inorganic, and carbon-based nanoparticles [157,158]. Different compositions and sizes of nanoparticles exhibit different functions, and hence can be adapted for specific electrochemical sensings, such as immunosensors, enzyme sensors, etc. [151,155,156]. Organic nanoparticles, such as micelles, liposomes, and dendrimers, are common organic nanoparticles with non-toxic and biodegradable properties. Nanocapsules (e.g., micelles and liposomes with hollow cores) are sensitive to thermal and electromagnetic radiation, such as light and heat [159]. Despite that, organic nanoparticles are popular in biomedical fields, especially drug delivery systems, because of their efficiency and ability to be injected into specific body parts [160].

Metal-based nanoparticles are inorganic nanoparticles produced from metal-based materials via constructive or destructive methods and practically almost all metals can be synthesized into specific nanoscale ranges [161]. To date, metal-based nanoparticles from gold (Au), iron (Fe), lead (Pb), aluminum (Al), cadmium (Cd), cobalt (Co), silver (Ag), and zinc (Zn) have been extensively studied for various biomedical applications [162–166]. Notable characteristics of metal-based nanoparticles include crystalline and amorphous structures, high surface area to volume ratio, pore size, surface charge density, sensitivity, and reactivity to environmental factors, such as sunlight, air, moisture, heat, etc. [167]. Metal nanoparticles are generally used as "electronic wires" to enhance electron transfer between an electrode's surface and redox centers in proteins because they have good conductivity. Moreover, these nanoparticles also present a good catalytic characteristic as promising catalysts for improving and increasing electrochemical reactions. For instance, Au nanoparticles or AuNP were integrated into IDEA by Sharma et al. [168]. However, Sharma and colleagues reported that one of the downsides of incorporating AuNPs into IDEA was a corrosion problem upon contact between the metal-based nanoparticles and electrolytes, confirmed via CV. In this case, considerable attention has been directed toward integrating carbon with metal electrodes for IDEA to curb the aforementioned problem.

Metal oxide-based nanoparticles [169] are developed to tackle the drawbacks of metal-based nanoparticles. For instance, in the presence of oxygen at room temperature, iron oxide (Fe_2O_3) is oxidized from iron (Fe) nanoparticles, thus, increasing its efficiency and reactivity, compared to iron nanoparticles [7]. Examples of common metal oxide-based nanoparticles are iron oxide (Fe_2O_3), zinc oxide (ZnO), magnetite (Fe_3O_4), silicon dioxide (SiO_2), aluminum oxide (Al_2O_3), cerium oxide (CeO_2), titanium oxide (TiO_2), and many more [170–172]. As such, magnetic iron oxide nanoparticles (IONPs) have been used for tumour-targeted gene delivery [173], owing to their propitious properties, such as ease of chemical functionalization, high biocompatibility, low toxicity, direct synthesis methods, and superior magnetic responsiveness [174–177].

Despite the mentioned advantages of carbon-based IDEA, its electrical conductivity is slightly lower than most metal-based IDEAs [178], resulting in a lower electrochemical performance. Therefore, complementary materials, such as gold nanoparticles (AuNPs), may help to enhance biosensor performance by facilitating the electron transfer and conductivity of the electrode to increase analytical selectivity and sensitivity. Gold nanoparticle-based IDEAs provide great advantages, such as chemical stability, quantum size effects, and ease of

synthesis advantageous for electronics, catalytic, and optical characteristics. Moreover, the high surface-to-volume ratio of AuNPs increases several magnitudes in electroactive surfaces, leading to high sensitivity and higher enzyme loading within the integrated devices [179].

The addition of AuNPs to IDEA has been studied by Sharma et al. [168] in which they dispersed the AuNPs on top of a 3D carbon IDEA. Furthermore, the fabricated glassy 3D carbon IDEA (3D C-IDEA) was composed of SU-8 2002 on SiO_2/Si wafer achieved via C-MEMS process with an aspect ratio of 1:1 to obtain 620 nm width, 650 nm height, and a gap between the adjacent comb of 1.9 µm. The fabricated AuNP/3D C-IDEA was prepared for cholesterol detection; hence, cholesterol oxidase (ChOx) was selectively immobilized on the AuNP/3D C-IDEA via electrochemical reduction of the diazonium cation. They analyzed the sensitivity of the AuNP/3D C-IDEA-based cholesterol biosensor via amplification of redox mediators between the combs of AuNP/3D C-IDEAs and immobilized enzymes area. The results were categorized as functionalized and non-functionalized with a wide sensing range (0.005–10 mM). The AuNP/3D C-IDEAs biosensor recorded lowest the LOD value (~1.28 µM) with high sensitivity (~993.91 µA mM^{-1} cm^{-2}), as compared to bare carbon IDEAs with an LOD of 4.15 µM and a sensitivity of 790.75 µA mM^{-1} cm^{-2}. Thus, the alteration of carbon IDEA with AuNP demonstrated enhanced sensor sensitivity and lower LOD values too.

The exciting combination between metal-based IDEA and nanomaterials towards innovative biosensing platforms stimulate an interesting piece of research led by Wiederoder et al. [180]. In this work, the research group prepared IDEA patterns with a combination of Cr/Au IDEA and porous sensor elements in the microfluidic channel. The preparation of the porous sensor in this work involved the functionalization of a packed bed of silica beads with antibody probes within a thermoplastic microchannel. The porous sensor element was completed with gold-based IDEA for further analysis by measuring the impedance changes in the concentration-dependent formation of silver aggregates, as illustrated in Figure 10. The 10 µm wide electrodes spaced 15, 40, and 100 µm apart within a 150 µm deep channel of IDEA's sensors were tested with silica beads functionalized with anti-human rabbit IgG to determine the best electrode geometries. According to their test results, the spacing of 100 µm was shown to be the best IDEA for further experiments. They also conducted an immunoassay test by introducing the AuNP anti-rabbit conjugates followed by silver enhancement. Based on the impedance measurement results, all positive test samples were confirmed through the changes of a white porous silica bead bed to a red-brown color, which was also in agreement with previous studies [181]. Their fabricated device with low-resolution electrodes expressed a detection limit, ranging between 1 and 10 ng/mL with a 4-log dynamic range for sandwich immunoassay and total assay time of 75 min. The limit of detection of 10 ng/mL for the IgG model system was achieved. Compared to the planar biosensors that require serial functionalization of individual devices, the silica beads used in this experiment are advantageous in terms of off-chip functionalization for greater manufacturability. In addition, it offers the possibility of using the packing of multiple beads for the development of various target probes.

4.3. Summary of IDEA-Based Electrochemical Sensors

IDEA-based electrochemical sensors have been reviewed in many aspects due to their popularity. As such, Afsarimanesh et al. elaborate on planar IDEA sensors linked to many types of signal-conditioning circuits and their application in biomedical, environmental, and industrial sectors [21]. Forouzanfar et al. discussed the technical aspect of the devices fabricated using C-MEMS and C-NEMS from photolithography and non-photolithography techniques, specifically for biotech applications [118]. Brosel-Oliu et al. reviewed the IDEA using an impedance technique for a variety of bacteria detection explicitly in terms of bacterial growth monitoring and label-free specific bacteria [12]. Moreover, carbon-based microelectrodes for neurotransmitters have been published elsewhere [182]. Following extensive reviews by others, the practical application of IDEA-based electrochemical sensors, concentrating on unique IDEA structures as a method to increase the surface area and sensitivity of the sensor while maintaining the miniaturized size are presented in Table 3.

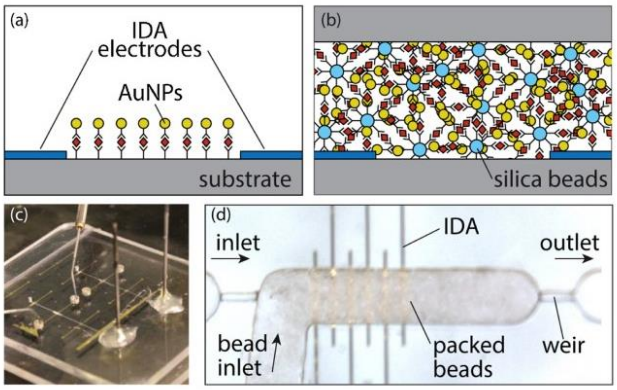

Figure 10. Idealized views of: (**a**) planar; (**b**) a volumetric impedimetric immunosensor; (**c**) fabricated thermoplastic device; and (**d**) magnified view of the detection zone, including thin-film gold IDEA and packed bed of functionalized silica beads in a 150 µm deep channel. Reprinted from [180], Copyright 2016, with permission from Elsevier.

Table 3. IDEA based-electrochemical sensor in biomedical applications using amperometric and impedimetric detections.

Techniques	Substrate/Electrode Materials	IDEA Dimensions	IDEA Structure	Sensor Performance	Ref.
Amperometric	Pt	w = g = h = 100 nm	Pt-nIDEA	AF = 161 for FcMeOH, CE = 99% -no biosensing test	[18]
Impedimetric	Polyimide sheet	w = 917 µm, g = 553 µm		2.5 CFU/mL of E. Coli detection	[102]
Impedimetric	Au	w = g = 10 µm, h = ~60 nm	PPy/CNT film on 2 Au 2D IDEA	LOD: 28 ng/mL CysC	[105]
Amperometric and Impedimetric	Fe	(a) w = 20 µm, g = 15 µm, h = 80 µm, (b) w = 25 µm, g = 25 µm, h = 5 µm, (c) w = 25 µm, g = 25 µm, h = 20 µm, and (d) w = 25 µm, g = 25 µm, h = 80 µm.	3D VACNT IDEA	LOD: 1 ng/mL F-biotin	[136]
Impedimetric	SU-8 2002, SU-8 2025	Suspended carbon mesh: w ~300 nm, IDEA g ~1.9 µm	Suspended carbon mesh on top of the 2D C-IDEA	LOD: 0.43 pg/mL cMyo human serum	[139]
Amperometric, chronocoulometric	ITO	w = 5 µm, g = 10 µm between the bottom and ceiling and h = several tens µm	Closed 2D IDEA and 3D IDEA	LOD: 10 fg/mL (3D IDEA) and ~100 fg/mL (Closed-2D IDEA) for mouseIgG 3D IDEA: 100 fg/mL for cTnI	[141]
Amperometric, Impedimetric	ITO electrode modified with PMG and PDA	w = 5 µm, g = 10 µm, h = 30 µm	3D IDEA without reference and counter electrodes.	LOD: 0.32 pg/mL of Creatine Kinase-MB	[146]
Amperometric and Impedimetric	Fe	w = g = 25 µm, h = 75 µm	3D VACNT IDEA	LOD: 0.24 pg/mL of CIP2A in salivasupernatant	[151]
Amperometric	SU-8 2002	w = 620 nm, h = 650 nm and g = 1.9 µm	AuNPs on top of 3D C-IDEA	LOD: ~1.28 µM of cholesterol	[168]
Impedimetric	Cr/Au	w = 10 µm, g = 100 µm	2D IDEA with porous sensor on top	LOD: 10 ng/mL for an IgG	[180]
Conductometric	Au	w = g = 20 µm	2D IDEA	LOD: 15 µM of ATP	[183]

5. Challenges and Future Directions

The COVID-19 pandemic has shown that our world is very susceptible to the chaos caused by biological threats, notwithstanding the innumerable improvements in biosensor technologies every year. Current rapid biosensors still suffer from shortcomings concerning sensitivity and specificity for accurate detection and analysis. Despite numerous publications on IDEA-based biosensors with various widths, gaps, and heights fabricated from several fabrication methods, these exciting biosensing devices are still in need of improvements to circumvent several limitations. In this literature, we summarized several challenges and future directions for upcoming IDEA-based electrochemical sensors.

5.1. Applications of IDEA-Based Sensors

Several ways to improve the IDEA-based electrochemical sensor performances have been discussed in the previous section, such as increasing the surface area of IDEA, the integration of nanocomposites, nanoparticles, and many more. In addition to the IDEA-based electrochemical sensors, Table 4 listed some applications of IDEA-based sensors between 2021 and 2022 to showcase the integration of IDEA with various materials to enhance the sensor performances for numerous applications.

Table 4. Integration of IDEA with nanomaterials and various source materials for wide ranging applications between years 2021 and 2022.

IDEA Source Materials	Integration in IDEA	Applications	Sensor Performance	Ref.
Ti/Pt IDEA	CuO–ZnO radial core–shell heterojunction nanowire arrays on metallic IDEA	photodetectors	responsivity: 26.3 A/W, detectivity: 5.8 × 1013 Jones	[184]
Metal IDEA on PET substrates	grown zinc oxide nanorod (NR) arrays cross-linked with IDEA	bending detection characteristics and sensing mechanism	no plasma treatment: highest gauge factor of 196 at a bending strain of 1.75% in the convex direction	[185]
C-Pt-IDEA	TiO_2 nanoparticles	photoelectrochemical (PEC) water splitting	shining of 365 nm LED light	[186]
Ti/Pt IDEA onglass substrates	one IDEA activated by enzyme immobilization with HRP	capacitive detection of the H_2O_2 vapor/aerosol	sensitivity of 57.8 nF/c(H_2O_2), the response time (<60 s)	[187]
$TaSi_2$ 3D-IDEA	with 4 µm high insulating barriers	detection of cyanobacteria cells	LOD: 100 cells·mL^{-1}	[188]
Au-IDEA	carbon nanodiamond	detection of SARS-CoV-2 nucleocapsid protein (NCP)	LOD: 0.389 fM	[189]
IDEA on polycarbonate substrates to make printed capacitive sensors	Ag nanoparticles	automotive infotainment	capacitance is increased when thickness increases	[190]
IDEA on ITO glass	carbon aerogel (CA)-polyaniline (PANI) composites	H_2S gas sensing	PANI-CA-3 sensitivity:452%	[191]
3D IDEA micro-supercapacitors (MSCs)	Si/C/CNT@TiC composite nanostructure	alternating current line filtering	capacitance: 7.42 mF cm^{-2} (3.71 F g^{-1}) at 5 mV s^{-1}	[192]
IDEA capacitor on woven fabric	-	tactile sensor	capacitance change-1.28 pF/gm.	[193]

5.2. Electrode Material

One of the struggles with fabricating the desired IDEA-based electrochemical sensors is related to the materials. Material selection to produce IDEA is vital because each material exhibits distinctive properties. The prerequisite characteristics of the best materials for IDEA should comply with the IDEA's application paradigms. Up to now, research into

the electrode materials of metal or carbon-MEMS IDEA-based electrochemical sensors has been extensively directed toward enhancing sensor sensitivity and selectivity. Metal/noble metal has been proven to exhibit excellent electrical conductivity, compared to pure carbon. However, some of the shortcomings of the noble metal include: (1) exhibiting unwanted electrochemical side reactions even at low potentials, and (2) corrosion upon contact with an electrolyte, for instance, Ti–Au or Cr–Au bilayers generate a galvanic couple and eventually corrosion [97]. In addition, some of the common noble metals for IDEA, e.g., Pt and Au need an adhesion layer, such as Ti or Cr, due to their weaker adhesion property onto Si or glass substrates. Nevertheless, metallic IDEAs have shown higher amplification factors, in contrast to other substrates, as presented in Table 3. Although Au possesses many advantages, such as high reliability and excellent electrical conductivity, it is not cost-effective and is easily diffused into substrates at low temperatures [94].

One of the main challenges in producing high-quality carbon IDEA is that poor conductivity of carbon may result in a large voltage drop. This hinders the miniaturizing of carbon MEMS electrodes to submicron ranges as resistance became overwhelmed in a small feature dimension [45,194–197]. Another challenge is the weak adhesion interface between the carbon layer and the substrate [45,195,197]. From this review, the integration of carbon and metal for IDEA's electrode has been explored for a better sensor performance [120,168] to ultimately achieve a higher amplification factor and collection efficiency and lower limits of detection while maintaining the miniaturized size of IDEA-based sensors.

5.3. Optimization of the Fabrication Process

Among the fabrication methods of IDEAs, C-MEMS offers one of the simplest fabrications with fewer steps of photolithography followed by pyrolysis. Despite that, the price of devices fabricated using this technique is not cost-effective for the end users. Mass production of metal-based IDEAs can be challenging due to complicated fabrication processes. In this case, C-MEMS is better candidate due to the simplicity of the fabrication steps. In addition to the fabrication techniques, the standardization of process parameters plays an important role in the sensitivity and effectiveness of the carbon IDEA-based sensor prototypes for reproducibility. Mamishev et al. mentioned that environmental working conditions, such as acidity, economic value, temperature, pressure, and the drawback of parameter estimation algorithms, may limit certain electrode structures [198]. For example, methods for fabrication processes, such as UV photolithography [199] and pyrolysis [200,201], require the optimization of exposure time and temperature, which will influence the final electrode properties, etc. Chemical or physical vapor deposition is one of the high-cost methods for metal deposition. In addition to metal deposition, the lift-off step that followed is expected to leave metal residue on the substrate surfaces [97]. Thus, micrometers/sub-micrometer parameters that can affect the biosensor performance should be controlled for the large-scale production of biosensors [21,49].

5.4. Modification of Planar IDEAs to 3D IDEAs

This review reveals that the modification of 2D IDEA to 3D IDEA is not limited to increasing thickness to obtain the desired height of the IDEA's fingers. Interestingly, increasing the surface area of the entire 3D IDEA has resulted in increased sensitivity of the sensor, which is a good indicator for building up an electrochemical sensor for various applications. In addition, the research on 2D and 3D IDEAs are expanding and focusing on the improvement of their performance and sensitivity while still maintaining micrometer or nanometer dimension. Current research is focusing on modifying and increasing the 3D IDEA surface area in order to obtain the higher sensitivity. Furthermore, the integration of microchannel as a method to increase the sensor surface area is quite exciting due to the different heights affecting the overall sensor reading. Studies related to the electrical double layer with or without the presence of the microchannels and flow or no-flow conditions within IDEA's sensing space require detailed analysis not only limited to the source of the IDEA's electrode materials but also the channel material [202,203].

Conversely, the build-up of 3D IDEA's space can be explored further through the study of the interaction between its unique design, such as suspending 3D IDEA with a combination of different metal electrode materials because the materials orchestrate distinctive characteristics upon contact with electrolytes or application tests. Fascinatingly, the two-electrode system (2E) from IDEA's design without the presence of the reference and counter electrodes, unlike the four-electrode configuration system, exhibit comparable results. Thus, further study on the IDEA's width, gap, height, expanded surface area, integration of nanoparticles, suspended carbon mesh, metal IDEA base layer, and many more for the purpose of producing carbon 3D IDEA are recommended for future works.

5.5. Reproducibility and Commercialization of IDEAs

Even though IDEAs are widely used in research for various advanced biosensors/sensors, limited number of promising sensors reached commercialization. One of the hindrances of transferring rapid biosensor technology from the lab to the commercial setting is batch-to-batch reproducibility. As the physiological samples are widely different, it is important to prevent the biosensor from reacting with other molecules from the samples using blocking agents. In addition, improvement of the sensor reproducibility for commercialization must focus on the automation of material handling. Automation allows full control of the equipment, particularly in the setting and production of the materials in a large scale production, e.g., the mixing process of high viscosity SU-8 2100 with cyclopentanone. Reagent dispensing using robotic pipettes onto the electrodes, etc., at the commercialization stage should be prioritized. The vast and fast production of small-sized sensors require accuracy at every fabrication stage. For example, the use of robotic pipettes may help to expedite the whole production process with minimal-to-zero dispensing errors. A controlled cleanroom facility for medical device manufacturing is the highest priority for upscaling manufacturing. Proper rules, regulations, frequent inspections by certified authorities for the overall manufacturing process should be implemented according to international laws. The regulations guidance for cleanroom space and the types of equipment are important for sensor/biosensor standardization and effectiveness in any application. It is also important to assess the global environmental impacts of mass production of biosensors, despite strict compliance with the standard protocols. Moreover, the integration of advanced telerobotic technologies for biosensor application testing will also have a huge impact on human healthcare as biosensor testing (e.g., dangerous viruses, such as COVID-19) can be performed remotely. Thus, the focus on the reproducibility and sustainability of IDEA biosensors is essential for successful commercialization.

6. Conclusions

The fabrication of IDEA-based electrochemical sensors is an evolving area of research because the biosensors/sensors configurations from three-electrode systems to four-electrode systems can be easily tailored via IDEA configuration. The unique design of IDEA makes it possible to be manipulated from planar IDEA to 3D IDEA via one of the simple fabrication methods, such as C-MEMS. The carbon-based MEMS method is straightforward, easy to fabricate, cost-effective, and reproducible. Furthermore, the carbon IDEAs based on carbon MEMS possess good criteria, such as high biocompatibility, good physicochemical characteristics, excellent chemical resistance, and stability for electrochemical measurements. This leads to high redox cycling efficiency due to the controllability of the carbon aspect ratios [50,83,204]. Carbon 2D IDEA is limited to low-signal amplification, unlike carbon 3D IDEA and metal IDEA/3D IDEA. The advantages of metal-based IDEAs include having very high amplification factors despite complex fabrication steps, compared to the C-MEMS method. A vast number of publications on IDEA-based electrochemical sensors reported a variation in 3D IDEA in terms of the width, height, and gap between adjacent fingers dimension, all of which increase the sensitivity of the sensors. Interestingly, in this review, several methods for increasing the 3D IDEA's surface area are highlighted, such as microchannel insertion, unique IDEA's structure (e.g., carbon pillar, the suspended

carbon), VACNT, nanoparticles integration using MEMS and other methods. Moreover, the integration of mesh and microchannel on IDEA constrains the electrolyte in a limited space while retaining the good electrical double layer effect in the overall IDEA's space. The combination of the carbon and metal/nanoparticle on the IDEA's structure may also escalate the resultant surface area and sensitivity of IDEA-based electrochemical sensors. The increase in the IDEA's surface area has shown better sensor sensitivity, compared to the basic 3D IDEA as it not only increases the height of the 3D IDEA but also expands the space for redox cycling. Moreover, miniaturized IDEAs are compatible with lab-on-chip devices for point-of-care testing systems. Despite the absence of reference and counter electrodes, IDEA's modification as a two-electrode system presented comparable results to the four-electrode configuration system, proving that the IDEA's unique design can be explored further for future IDEA-based electrochemical sensors. The authors of this review believe that the modification of carbon–IDEA designs with combination of carbon and metal IDEA-based electrochemical sensing techniques would be an ideal future research direction. These carbon–IDEA modification designs can deliver rapid and highly sensitive detection to chemical sensors for applications in food safety [205], homeland security [206], biomedical applications [207], environmental sensing [21], and industrial applications, among many others.

Author Contributions: E.K. contributed to the investigation, writing of the original draft, reviewing of the manuscript, and preparation of the figures. A.T., F.I. and M.M. provided supervision and reviewed the manuscript. Grant and project administered by F.I. All authors have read and agreed to the published version of the manuscript.

Funding: This research was funded by Ministry of Science and Technology (MOSTI) (MOSTI002B-2022TED1), Ministry of Higher Education (MOHE) and Universiti Malaya under grant TU003-2019 and IIRG007A-19HWB.

Institutional Review Board Statement: Not applicable.

Informed Consent Statement: Not applicable.

Data Availability Statement: Not applicable.

Acknowledgments: The authors would like to acknowledge Ministry of Science and Technology (MOSTI) (MOSTI002B-2022TED1) for financial support. This research was also funded by the Ministry of Higher Education (MOHE) and Universiti Malaya under TU003-2019 and IIRG007A-19HWB. The authors would also like to thank Nuraina Anisa Dahlan for proofreading this manuscript.

Conflicts of Interest: The authors declare no conflict of interest.

References

1. Morrison, D.W.G.; Dokmeci, M.; Demirci, U.; Khademhosseini, A. Clinical Applications of Micro- and Nanoscale Biosensors. In *Biomedical Nanostructures*; Gonsalves, K.E., Laurencin, C.L., Halberstadt, C.R., Nair, L.S., Eds.; John Wiley & Sons, Inc.: Toronto, ON, Canada, 2008.
2. Kahn, K.; Plaxco, K.W. Principles of biomolecular recognition. In *Recognition Receptors in Biosensors*; Zourob, M., Ed.; Springer: New York, NY, 2010; pp. 3–45. [CrossRef]
3. Lowe, C.R. Overview of Biosensor and Bioarray Technologies. In *Handbook of Biosensors and Biochips*; Wiley: Hoboken, NJ, USA, 2008. [CrossRef]
4. Perumal, V.; Hashim, U. Advances in biosensors: Principle, architecture and applications. *J. Appl. Biomed.* **2014**, *12*, 1–15. [CrossRef]
5. Velusamy, V.; Arshak, K.; Korostynska, O.; Oliwa, K.; Adley, C. An overview of foodborne pathogen detection: In the perspective of biosensors. *Biotechnol. Adv.* **2010**, *28*, 232–254. [CrossRef] [PubMed]
6. Muniandy, S.; Teh, S.J.; Thong, K.L.; Thiha, A.; Dinshaw, I.J.; Lai, C.W.; Ibrahim, F.; Leo, B.F. Carbon Nanomaterial-Based Electrochemical Biosensors for Foodborne Bacterial Detection. *Crit. Rev. Anal. Chem.* **2019**, *49*, 510–533. [CrossRef] [PubMed]
7. Chaubey, A.; Malhotra, B.D. Mediated biosensors. *Biosens. Biolelectron.* **2002**, *17*, 441–456. [CrossRef] [PubMed]
8. Tothill, I.E. Biosensors and nanomaterials and their application for mycotoxin determination. *World Mycotoxin J.* **2011**, *4*, 361–374. [CrossRef]
9. Berrettoni, M.; Tonelli, D.; Conti, P.; Marassi, R.; Trevisani, M. Electrochemical sensor for indirect detection of bacterial population. *Sens. Actuators B Chem.* **2004**, *102*, 331–335. [CrossRef]

10. Ronkainen, N.J.; Halsall, H.B.; Heineman, R.W. Electrochemical biosensors. *Chem. Soc. Rev.* **2010**, *39*, 1747–1763. [CrossRef]
11. Brosel-Oliu, S.; Ferreira, R.; Uria, N.; Abramova, N.; Gargallo, R.; Muñoz-Pascual, F.-X.; Bratov, A. Novel impedimetric aptasensor for label-free detection of *Escherichia coli* O157:H7. *Sens. Actuators B Chem.* **2018**, *255*, 2988–2995. [CrossRef]
12. Brosel-Oliu, S.; Abramova, N.; Uria, N.; Bratov, A. Impedimetric transducers based on interdigitated electrode arrays for bacterial detection—A review. *Anal. Chim. Acta* **2019**, *1088*, 1–19. [CrossRef]
13. Li, L.; Chen, Z.; Wang, S.; Jin, X.; Yang, L.; Liu, G.; Zhao, J. Highly selective detection of *Escherichia coli* O157:H7 based on micro-gapped interdigitated electrode arrays. *Biotechnol. Biotechnol. Equip.* **2017**, *31*, 1070–1078. [CrossRef]
14. Maalouf, R.; Fournier-Wirth, C.; Coste, J.; Chebib, H.; Saïkali, Y.; Vittori, O.; Errachid, A.; Cloarec, J.-P.; Martelet, C.; Jaffrezic-Renault, N. Label-Free Detection of Bacteria by Electrochemical Impedance Spectroscopy: Comparison to Surface Plasmon Resonance. *Anal. Chem.* **2007**, *79*, 4879–4886. [CrossRef]
15. Abdalhai, M.H.; Fernandes, A.M.; Xia, X.; Musa, A.; Ji, J.; Sun, X. Electrochemical Genosensor To Detect Pathogenic Bacteria (*Escherichia coli* O157:H7) As Applied in Real Food Samples (Fresh Beef) To Improve Food Safety and Quality Control. *J. Agric. Food Chem.* **2015**, *63*, 5017–5025. [CrossRef]
16. Grieshaber, D.; MacKenzie, R.; Voeroes, J.; Reimhult, E. Electrochemical biosensors—Sensor principles and architectures. *Sensors* **2008**, *8*, 1400–1458. [CrossRef]
17. Power, A.C.; Gorey, B.; Chandra, S.; Chapman, J. Carbon nanomaterials and their application to electrochemical sensors: A review. *Nanotechnol. Rev.* **2018**, *7*, 19–41. [CrossRef]
18. Matylitskaya, V.; Kasemann, S.; Urban, G.; Dincer, C.; Partel, S. Electrochemical Characterization of Nanogap Interdigitated Electrode Arrays for Lab-on-a-Chip Applications. *J. Electrochem. Soc.* **2018**, *165*, B127–B134. [CrossRef]
19. Alayo, N.; Fernández-Sánchez, C.; Baldi, A.; Esquivel, J.P.; Borrisé, X.; Pérez-Murano, F. Gold interdigitated nanoelectrodes as a sensitive analytical tool for selective detection of electroactive species via redox cycling. *Microchim. Acta* **2016**, *183*, 1633–1639. [CrossRef]
20. Ben Ali, M.; Korpan, Y.; Gonchar, M.; El'Skaya, A.; Maaref, M.; Jaffrezic-Renault, N.; Martelet, C. Formaldehyde assay by capacitance versus voltage and impedance measurements using bi-layer bio-recognition membrane. *Biosens. Bioelectron.* **2006**, *22*, 575–581. [CrossRef]
21. Afsarimanesh, N.; Nag, A.; Alahi, M.E.E.; Han, T.; Mukhopadhyay, S. Interdigital sensors: Biomedical, environmental and industrial applications. *Sens. Actuators A Phys.* **2020**, *305*, 111923. [CrossRef]
22. Sophocleous, M.; Atkinson, J.K. A review of screen-printed silver/silver chloride (Ag/AgCl) reference electrodes potentially suitable for environmental potentiometric sensors. *Sens. Actuators A Phys.* **2017**, *267*, 106–120. [CrossRef]
23. Michalska, A.; Kisiel, A.; Maksymiuk, K. Screen-Printed Disposable Reference Electrodes. In *Handbook of Reference Electrodes*; Springer: Berlin, Heidelberg, Germany, 2013; pp. 325–330. [CrossRef]
24. Khan, M.; Rahaman, R.; Khalilian, A.; Kang, S.-W. Fast, highly-sensitive, and wide-dynamic-range interdigitated capacitor glucose biosensor using solvatochromic dye-containing sensing membrane. *Sensors* **2016**, *16*, 265. [CrossRef]
25. Lee, G.H.; Pyun, J.-C.; Cho, S. Electrical impedance characterization of cell growth on interdigitated microelectrode array. *J. Nanosci. Nanotechnol.* **2014**, *14*, 8342–8346. [CrossRef] [PubMed]
26. Banga, I.; Paul, A.; France, K.; Micklich, B.; Cardwell, B.; Micklich, C.; Prasad, S.E.C. Tech-electrochemical handheld breathalyzer COVID sensing technology. *Sci. Rep.* **2022**, *12*, 4370. [CrossRef] [PubMed]
27. Sheppard, N.F.; Tucker, R.C.; Wu, C. Electrical conductivity measurements using microfabricated interdigitated electrodes. *Anal. Chem.* **1993**, *65*, 1199–1202. [CrossRef]
28. Iwasaki, Y.; Morita, M. Electrochemical measurements with interdigitated array microelectrodes. *Curr. Sep.* **1995**, *14*, 2–8.
29. Dizon, A.; Orazem, M.E. On the impedance response of interdigitated electrodes. *Electrochim. Acta* **2019**, *327*, 135000. [CrossRef]
30. Barnes, E.O.; Lewis, G.E.M.; Dale, S.; Marken, F.; Compton, R.G. Generator-collector double electrode systems: A review. *Analyst* **2012**, *137*, 1068–1081. [CrossRef]
31. Tomčík, P.; Bustin, D. Voltammetric determination of iodide by use of an interdigitated microelectrode array. *Fresenius J. Anal. Chem.* **2001**, *371*, 562–564. [CrossRef]
32. Bustin, D.; Jursa, S.; Tomčík, P. Titrations with electrogenerated halogens in the diffusion layer of an interdigitated microelectrode array. *Analyst* **1996**, *121*, 1795–1799. [CrossRef]
33. McAdams, E.; Lackermeier, A.; McLaughlin, J.; Macken, D.; Jossinet, J. The linear and non-linear electrical properties of the electrode-electrolyte interface. *Biosens. Bioelectron.* **1995**, *10*, 67–74. [CrossRef]
34. Bandarenka, A.S. Exploring the interfaces between metal electrodes and aqueous electrolytes with electrochemical impedance spectroscopy. *Analyst* **2013**, *138*, 5540–5554. [CrossRef]
35. Yun, J.; Kang, G.; Park, Y.; Kim, H.W.; Cha, J.-J.; Lee, J.-H. Electrochemical impedance spectroscopy with interdigitated electrodes at the end of hypodermic needle for depth profiling of biotissues. *Sens. Actuators B Chem.* **2016**, *237*, 984–991. [CrossRef]
36. Kuo, Y.-C.; Lee, C.-K.; Lin, C.-T. Improving sensitivity of a miniaturized label-free electrochemical biosensor using zigzag electrodes. *Biosens. Bioelectron.* **2018**, *103*, 130–137. [CrossRef]
37. Nadzirah, S.; Hashim, U. Interdigitated microelectrode geometry for simple electrical *Escherichia coli* O157:H7 DNA detection. *Microelectron. Int.* **2017**, *34*, 99–107. [CrossRef]

38. Cheng, Y.H.; Moura, P.A.R.; Zhenglong, L.; Feng, L.; Arokiam, S.; Yang, J.; Hariharan, M.; Basuray, S. Effect of electrode configuration on the sensitivity of nucleic acid detection in a non-planar, flow-through, porous interdigitated electrode. *Biomicrofluidics* **2019**, *13*, 064118. [CrossRef]
39. Muaz, A.; Hashim, U.; Liu, W.-W.; Ibrahim, F.; Thong, K.; Mohktar, M.S. Fabrication of interdigitated electrodes (IDE's) by conventional photolithography technique for pH measurement using micro-gap structure. In Proceedings of the 2014 IEEE Conference on Biomedical Engineering and Sciences (IECBES), Kuala Lumpur, Malaysia, 8–10 December 2014; pp. 146–150. [CrossRef]
40. Gondosiswanto, R.; Hibbert, D.B.; Fang, Y.; Zhao, C. Redox Recycling Amplification Using an Interdigitated Microelectrode Array for Ionic Liquid-Based Oxygen Sensors. *Anal. Chem.* **2018**, *90*, 3950–3957. [CrossRef]
41. Bratov, A.; Ramón-Azcón, J.; Abramova, N.; Merlos, A.; Adrian, J.; Sánchez-Baeza, F.; Marco, M.-P.; Dominguez, C. Three-dimensional interdigitated electrode array as a transducer for label-free biosensors. *Biosens. Bioelectron.* **2008**, *24*, 729–735. [CrossRef]
42. Lequin, R.M. Enzyme Immunoassay (EIA)/Enzyme-Linked Immunosorbent Assay (ELISA). *Clin. Chem.* **2005**, *51*, 2415–2418. [CrossRef]
43. Niwa, O.; Morita, M.; Tabei, H. Fabrication and characteristics of vertically separated interdigitated array electrodes. *J. Electroanal. Chem. Interfacial Electrochem.* **1989**, *267*, 291–297. [CrossRef]
44. Horiuchi, T.; Niwa, O.; Morita, M.; Tabei, H. Quantitative analysis of the steady-state currents of reversible redox species at a microdisk array electrode embedded in a surface electrode. *J. Electroanal. Chem. Interfacial Electrochem.* **1990**, *295*, 25–40. [CrossRef]
45. Morita, M.; Niwa, O.; Horiuchi, T. Interdigitated array microelectrodes as electrochemical sensors. *Electrochim. Acta* **1997**, *42*, 3177–3183. [CrossRef]
46. Zafarani, H.R.; Mathwig, K.; Sudhölter, E.J.; Rassaei, L. Electrochemical redox cycling in a new nanogap sensor: Design and simulation. *J. Electroanal. Chem.* **2016**, *760*, 42–47. [CrossRef]
47. Aoki, K.; Morita, M.; Niwa, O.; Tabei, H. Quantitative analysis of reversible diffusion-controlled currents of redox soluble species at interdigitated array electrodes under steady-state conditions. *J. Electroanal. Chem. Interfacial Electrochem.* **1988**, *256*, 269–282. [CrossRef]
48. Bard, A.J.; Crayston, J.A.; Kittlesen, G.P.; Varco Shea, T.; Wrighton, M.S. Digital simulation of the measured electrochemical response of reversible redox couples at microelectrode arrays: Consequences arising from closely spaced ultramicroelectrodes. *Anal. Chem.* **1986**, *58*, 2321–2331. [CrossRef]
49. Heo, J.-I.; Lim, Y.; Shin, H. The effect of channel height and electrode aspect ratio on redox cycling at carbon interdigitated array nanoelectrodes confined in a microchannel. *Analyst* **2013**, *138*, 6404–6411. [CrossRef] [PubMed]
50. Heo, J.I.; Shim, D.S.; Teixidor, G.T.; Oh, S.; Madou, M.J.; Shin, H. Carbon Interdigitated Array Nanoelectrodes for Electrochemical Applications. *J. Electrochem. Soc.* **2011**, *158*, J76–J80. [CrossRef]
51. Sugime, H.; Ushiyama, T.; Nishimura, K.; Ohno, Y.; Noda, S. An interdigitated electrode with dense carbon nanotube forests on conductive supports for electrochemical biosensors. *Analyst* **2018**, *143*, 3635–3642. [CrossRef]
52. Zevenbergen, M.A.G.; Wolfrum, B.L.; Goluch, E.D.; Singh, P.S.; Lemay, S.G. Fast Electron-Transfer Kinetics Probed in Nanofluidic Channels. *J. Am. Chem. Soc.* **2009**, *131*, 11471–11477. [CrossRef]
53. Varshney, M.; Li, Y.; Srinivasan, B.; Tung, S.J.S. A label-free, microfluidics and interdigitated array microelectrode-based impedance biosensor in combination with nanoparticles immunoseparation for detection of *Escherichia coli* O157: H7 in food samples. *Sens. Actuators B Chem.* **2007**, *128*, 99–107. [CrossRef]
54. Kamath, R.R.; Madou, M.J. Three-Dimensional Carbon Interdigitated Electrode Arrays for Redox-Amplification. *Anal. Chem.* **2014**, *86*, 2963–2971. [CrossRef]
55. Madou, M. *Fundamentals of Microfabrication: The Science of Miniaturization*; CRC: Boca Raton, FL, USA, 2002.
56. Madou, M.; Schmidt, G.; Song, X.; Kinoshita, K.; Fendorf, M.; Zettly, A.; White, R. Carbon micromachining (c-mems). In Proceedings of the Symposium on Chemical and Biological Sensors and Analytical Electrochemical Methods, Paris, France, 1 January 1997; The Electrochemical Society, Inc.: Pennington, NJ, USA; Volume 97, pp. 61–69.
57. Chikkaveeraiah, B.V.; Bhirde, A.A.; Morgan, N.Y.; Eden, H.S.; Chen, X. Electrochemical Immunosensors for Detection of Cancer Protein Biomarkers. *ACS Nano* **2012**, *6*, 6546–6561. [CrossRef]
58. Rocchitta, G.; Spanu, A.; Babudieri, S.; Latte, G.; Madeddu, G.; Galleri, G.; Nuvoli, S.; Bagella, P.; Demartis, M.; Fiore, V. Analytical problems in exposing amperometric enzyme biosensors to biological fluids. *Sensors* **2016**, *16*, 780.
59. Sharma, N.K.; Nain, A.; Singh, K.; Rani, N.; Singal, A. Impedimetric Sensors: Principles, Applications and Recent Trends. *Int. J. Innov. Technol. Explor. Eng.* **2019**, *8*, 2278–3075. [CrossRef]
60. Bahadır, E.B.; Sezgintürk, M.K. A review on impedimetric biosensors. *Artif. Cells Nanomed. Biotechnol.* **2014**, *44*, 248–262. [CrossRef]
61. Jaffrezic-Renault, N.; Dzyadevych, S.V. Conductometric Microbiosensors for Environmental Monitoring. *Sensors* **2008**, *8*, 2569–2588. [CrossRef]
62. Stradiotto, N.; Yamanaka, H.; Zanoni, M.V.B. Electrochemical sensors: A powerful tool in analytical chemistry. *J. Braz. Chem. Soc.* **2003**, *14*, 159–173. [CrossRef]
63. Willander, M.; Tahira, A.; Ibupoto, Z. Potentiometric Biosensors Based on Metal Oxide Nanostructures. In *Encyclopedia of Interfacial Chemistry*; Elsevier: Amsterdam, The Netherlands, 2018. [CrossRef]

64. Grahame, D.C. The Electrical Double Layer and the Theory of Electrocapillarity. *Chem. Rev.* **1947**, *41*, 441–501. [CrossRef]
65. Smith, C.P.; White, H.S. Theory of the voltammetric response of electrodes of submicron dimensions. Violation of electroneutrality in the presence of excess supporting electrolyte. *Anal. Chem.* **1993**, *65*, 3343–3353. [CrossRef]
66. He, R.; Chen, S.; Yang, A.F.; Wu, B. Dynamic Diffuse Double-Layer Model for the Electrochemistry of Nanometer-Sized Electrodes. *J. Phys. Chem. B* **2006**, *110*, 3262–3270. [CrossRef]
67. Oldham, K.; Bond, A. How valid is the electroneutrality approximation in the theory of steady-state voltammetry? *J. Electroanal. Chem.* **2001**, *508*, 28–40. [CrossRef]
68. Yang, X.; Zhang, G. Simulating the structure and effect of the electrical double layer at nanometre electrodes. *Nanotechnology* **2007**, *18*, 335201. [CrossRef]
69. Yang, X.; Zhang, G. The effect of an electrical double layer on the voltammetric performance of nanoscale interdigitated electrodes: A simulation study. *Nanotechnology* **2008**, *19*, 465504. [CrossRef] [PubMed]
70. Bearden, S.L. *Manipulation of the Electrical Double Layer for Control and Sensing in a Solid State Nanopore*; Clemson University: Clemson, SC, USA, 2015.
71. Ngo, T.-T.; Shirzadfar, H.; Bourjilat, A.; Kourtiche, D.; Nadi, M. A method to determine the parameters of the double layer of a planar interdigital sensor. *Int. J. Smart Sens. Intell. Syst.* **2014**, *7*, 1–4. [CrossRef]
72. Fleischmann, M.; Pons, S.; Rolison, D.R. *Ultramicroelectrodes*; Datatech Systems: Birkenhead, UK, 1987.
73. Wightman, R.M. Microvoltammetric electrodes. *Anal. Chem.* **1981**, *53*, 1125A–1134A. [CrossRef]
74. Aoki, K.; Akimoto, K.; Tokuda, K.; Matsuda, H.; Osteryoung, J. Linear sweep voltammetry at very small stationary disk electrodes. *J. Electroanal. Chem. Interfacial Electrochem.* **1984**, *171*, 219–230. [CrossRef]
75. Wang, H.; Pilon, L. Accurate Simulations of Electric Double Layer Capacitance of Ultramicroelectrodes. *J. Phys. Chem. C* **2011**, *115*, 16711–16719. [CrossRef]
76. Yasuga, H.; Shoji, K.; Koiwai, K.; Kawano, R. New Sensing Technologies: Microtas/NEMS/MEMS. In *Encyclopedia of Sensors and Biosensors*; Elsevier: Amsterdam, The Netherlands, 2021. [CrossRef]
77. Li, D.; Batchelor-McAuley, C.; Chen, L.; Compton, R.G. Band Electrodes in Sensing Applications: Response Characteristics and Band Fabrication Methods. *ACS Sens.* **2019**, *4*, 2250–2266. [CrossRef]
78. Niwa, O.; Morita, M.; Tabei, H. Electrochemical behavior of reversible redox species at interdigitated array electrodes with different geometries: Consideration of redox cycling and collection efficiency. *Anal. Chem.* **1990**, *62*, 447–452. [CrossRef]
79. Huang, C.-W.; Lu, M.S.-C. Electrochemical Detection of the Neurotransmitter Dopamine by Nanoimprinted Interdigitated Electrodes and a CMOS Circuit With Enhanced Collection Efficiency. *IEEE Sens. J.* **2011**, *11*, 1826–1831. [CrossRef]
80. Rassaei, L.; Mathwig, K.; Kang, S.; Heering, H.A.; Lemay, S.G. Integrated Biodetection in a Nanofluidic Device. *ACS Nano* **2014**, *8*, 8278–8284. [CrossRef]
81. Bobade, S.; Kalorey, D.; Warke, S. Biosensor Devices: A review on their biological applications. *Biosci. Biotechnol. Res. Commun.* **2016**, *9*, 132–137. [CrossRef]
82. Piñón, M.V.; Benítez, B.C.; Pramanick, B.; Perez-Gonzalez, V.H.; Madou, M.J.; Martinez-Chapa, S.O.; Hwang, H. Direct current-induced breakdown to enhance reproducibility and performance of carbon-based interdigitated electrode arrays for AC electroosmotic micropumps. *Sens. Actuators A Phys.* **2017**, *262*, 10–17. [CrossRef]
83. Pramanick, B.; Vazquez-Pinon, M.; Torres-Castro, A.; Martinez-Chapaa, S.O.; Madou, M. Effect of pyrolysis process parameters on electrical, physical, chemical and electro-chemical properties of SU-8-derived carbon structures fabricated using the C-MEMS process. *Mater. Today Proc.* **2018**, *5*, 9669–9682. [CrossRef]
84. Martinez-Duarte, R. SU-8 Photolithography as a Toolbox for Carbon MEMS. *Micromachines* **2014**, *5*, 766–782. [CrossRef]
85. Wang, S.; Peng, T.; Meng, Q.; Zhu, X.; Guo, L.; Yao, K.; Wang, Z.; Zheng, P.; Ren, Z.; He, Z.; et al. Rapid and ultrasensitive detection of *Salmonella typhimurium* using a novel impedance biosensor based on SiO_2@MnO_2 nanocomposites and interdigitated array microelectrodes. *Sens. Actuators B Chem.* **2020**, *324*, 128654. [CrossRef]
86. Aliabadi, E.S. Carbon Interdigitated Electrode Arrays for Biosensing. Ph.D. Thesis, UC Irvine, Irvine, CA, USA, 2021.
87. Zou, Z.; Kai, J.; Rust, M.J.; Han, J.; Ahn, C.H. Functionalized nano interdigitated electrodes arrays on polymer with integrated microfluidics for direct bio-affinity sensing using impedimetric measurement. *Sens. Actuators A Phys.* **2007**, *136*, 518–526. [CrossRef]
88. Bhura, D.K. 3D Interdigitated Electrode Array (IDEA) Biosensor For Detection of Serum Biomarker. Master's Thesis, Portland State University, Portland, OR, USA, 2011. [CrossRef]
89. Webster, M.S.; Timoshkin, I.V.; Macgregor, S.J.; Mattey, M. Computer aided modelling of an interdigitated microelectrode array impedance biosensor for the detection of bacteria. *IEEE Trans. Dielectr. Electr. Insul.* **2009**, *16*, 1356–1363. [CrossRef]
90. Yuan, Q.; Yang, K.; Wu, J. Optimization of planar interdigitated microelectrode array for biofluid transport by AC electrothermal effect. *Microfluid. Nanofluid.* **2013**, *16*, 167–178. [CrossRef]
91. O'Sullivan, B.; Patella, B.; Daly, R.; Seymour, I.; Robinson, C.; Lovera, P.; Rohan, J.; Inguanta, R.; O'Riordan, A. A simulation and experimental study of electrochemical pH control at gold interdigitated electrode arrays. *Electrochim. Acta* **2021**, *395*, 139113. [CrossRef]
92. MacKay, S.; Hermansen, P.; Wishart, D.; Hiebert, W.; Chen, J. Simulating electrical properties of interdigitated electrode designs for impedance-based biosensing applications. In Proceedings of the 2015 IEEE 28th Canadian Conference on Electrical and Computer Engineering (CCECE), Halifax, NS, Canada, 3–6 May 2015; pp. 370–375. [CrossRef]

93. Lavacchi, A.; Bardi, U.; Borri, C.; Caporali, S.; Fossati, A.; Perissi, I. Cyclic voltammetry simulation at microelectrode arrays with COMSOL Multiphysics®. *J. Appl. Electrochem.* **2009**, *39*, 2159–2163. [CrossRef]
94. Jun, L.Q.; bin Djaswadi, G.W.; bin Hawari, H.F.; Zakariya, M.A.B. Simulation of interdigitated electrodes (IDEs) geometry using COMSOL Multiphysics. In Proceedings of the 2018 International Conference on Intelligent and Advanced System (ICIAS), Kuala Lumpur, Malaysia, 13–14 August 2018; pp. 1–6. [CrossRef]
95. Deshpande, S.; Bhand, S.; Bacher, G. Investigation of the effect of metallization ratio and side shift on the interdigitated electrodes performance for biochemical sensing. *J. Appl. Electrochem.* **2021**, *51*, 893–904. [CrossRef]
96. Lvovich, V.F.; Liu, C.; Smiechowski, M.F. Optimization and fabrication of planar interdigitated impedance sensors for highly resistive non-aqueous industrial fluids. *Sens. Actuators B Chem.* **2006**, *119*, 490–496. [CrossRef]
97. Madou, M.J.; Perez-Gonzalez, V.H.; Pramanick, B. *Carbon: The Next Silicon?: Book 2—Applications*; Momentum Press: New York, NY, USA, 2016.
98. Ghosh, P.; Han, G.; De, M.; Kim, C.K.; Rotello, V.M. Gold nanoparticles in delivery applications. *Adv. Drug Deliv. Rev.* **2008**, *60*, 1307–1315. [CrossRef] [PubMed]
99. Upadhyayula, V.K. Functionalized gold nanoparticle supported sensory mechanisms applied in detection of chemical and biological threat agents: A review. *Anal. Chim. Acta* **2012**, *715*, 1–18. [CrossRef] [PubMed]
100. Daniel, M.-C.; Astruc, D. Gold Nanoparticles: Assembly, Supramolecular Chemistry, Quantum-Size-Related Properties, and Applications toward Biology, Catalysis, and Nanotechnology. *Chem. Rev.* **2004**, *104*, 293–346. [CrossRef] [PubMed]
101. Saha, K.; Agasti, S.S.; Kim, C.; Li, X.; Rotello, V.M. Gold Nanoparticles in Chemical and Biological Sensing. *Chem. Rev.* **2012**, *112*, 2739–2779. [CrossRef]
102. Rishi, M.; Amreen, K.; Gohel, K.; Javed, A.; Dubey, S.K.; Goel, S. Three Different Rapidly Prototyped Polymeric Substrates with Interdigitated Electrodes for *Escherichia coli* Sensing: A Comparative Study. *IEEE Trans. NanoBiosci.* **2022**. [CrossRef]
103. Daly, R.; Narayan, T.; Shao, H.; O'Riordan, A.; Lovera, P. Platinum-Based Interdigitated Micro-Electrode Arrays for Reagent-Free Detection of Copper. *Sensors* **2021**, *21*, 3544. [CrossRef]
104. Hwang, C.; Park, N.; Kim, E.S.; Kim, M.; Kim, S.D.; Park, S.; Kim, N.Y.; Kim, J.H. Ultra-fast and recyclable DNA biosensor for point-of-care detection of SARS-CoV-2 (COVID-19). *Biosens. Bioelectron.* **2021**, *185*, 113177. [CrossRef]
105. Ferreira, P.A.; Araujo, M.C.; Prado, C.M.; de Lima, R.A.; Rodríguez, B.A.; Dutra, R.F. An ultrasensitive Cystatin C renal failure immunosensor based on a PPy/CNT electrochemical capacitor grafted on interdigitated electrode. *Colloids Surf. B Biointerfaces* **2020**, *189*, 110834. [CrossRef]
106. Oh, C.; Yang, L.; Park, B.; Bohn, P. Interdigitated Electrode Arrays for Electrochemical Immunosensing of Interleukin-6 in Cerebrospinal Fluid (CSF) and Serum. *ECS Meet. Abstr.* **2021**, *MA2021-01*, 1380. [CrossRef]
107. Wang, C.; Zaouk, R.; Park, B.Y.; Madou, M.J. Carbon as a MEMS material: Micro and nanofabrication of pyrolysed photoresist carbon. *Int. J. Manuf. Technol. Manag.* **2008**, *13*, 360. [CrossRef]
108. Shaw, J.M.; Gelorme, J.D.; Labianca, N.C.; Conley, W.E.; Holmes, S.J. Negative photoresists for optical lithography. *IBM J. Res. Dev.* **1997**, *41*, 81–94. [CrossRef]
109. Sanders, D.P. Advances in Patterning Materials for 193 nm Immersion Lithography. *Chem. Rev.* **2010**, *110*, 321–360. [CrossRef]
110. Ueno, K.; Hayashida, M.; Ye, J.-Y.; Misawa, H. Fabrication and electrochemical characterization of interdigitated nanoelectrode arrays. *Electrochem. Commun.* **2005**, *7*, 161–165. [CrossRef]
111. Moreau, W.M. *Semiconductor Lithography: Principles, Practices, and Materials*; Springer: Berlin/Heidelberg, Germany, 1988.
112. Elliott, D.J. *Integrated Circuit Fabrication Technology*; McGraw-Hill: New York, NY, USA, 1982.
113. Wang, C.; Jia, G.; Taherabadi, L.; Madou, M. A novel method for the fabrication of high-aspect ratio C-MEMS structures. *J. Microelectromech. Syst.* **2005**, *14*, 348–358. [CrossRef]
114. Forouzanfar, S.; Alam, F.; Pala, N.; Wang, C. Highly sensitive label-free electrochemical aptasensors based on photoresist derived carbon for cancer biomarker detection. *Biosens. Bioelectron.* **2020**, *170*, 112598. [CrossRef]
115. Vomero, M.; Zucchini, E.; Delfino, E.; Gueli, C.; Mondragon, N.C.; Carli, S.; Fadiga, L.; Stieglitz, T. Glassy Carbon Electrocorticography Electrodes on Ultra-Thin and Finger-Like Polyimide Substrate: Performance Evaluation Based on Different Electrode Diameters. *Materials* **2018**, *11*, 2486. [CrossRef]
116. Quang, L.N.; Larsen, P.E.; Boisen, A.; Keller, S.S. Tailoring stress in pyrolytic carbon for fabrication of nanomechanical string resonators. *Carbon* **2018**, *133*, 358–368. [CrossRef]
117. Kim, J.; Song, X.; Kinoshita, K.; Madou, M.; White, R. Electrochemical Studies of Carbon Films from Pyrolyzed Photoresist. *J. Electrochem. Soc.* **1998**, *145*, 2314–2319. [CrossRef]
118. Forouzanfar, S.; Pala, N.; Madou, M.; Wang, C. Perspectives on C-MEMS and C-NEMS biotech applications. *Biosens. Bioelectron.* **2021**, *180*, 113119. [CrossRef]
119. Liu, F.; Kolesov, G.; Parkinson, B.A. Preparation, Applications, and Digital Simulation of Carbon Interdigitated Array Electrodes. *Anal. Chem.* **2014**, *86*, 7391–7398. [CrossRef] [PubMed]
120. Liu, F.; Divan, R.; Parkinson, B.A. Fabrication of Carbon-Platinum Interdigitated Array Electrodes and Their Application for Investigating Homogeneous Hydrogen Evolution Catalysis. *J. Electrochem. Soc.* **2015**, *162*, H645–H650. [CrossRef]
121. Ueno, K.; Kim, H.-B.; Kitamura, N. Characteristic Electrochemical Responses of Polymer Microchannel−Microelectrode Chips. *Anal. Chem.* **2003**, *75*, 2086–2091. [CrossRef] [PubMed]

122. Ito, T.; Maruyama, K.; Sobue, K.; Ohya, S.; Niwa, O.; Suzuki, K. Electrochemical Behavior of Parallel Opposed Dual Electrode in a Microchannel. *Electroanalysis* **2004**, *16*, 2035–2041. [CrossRef]
123. Mathew, D.G.; Beekman, P.; Lemay, S.G.; Zuilhof, H.; Le Gac, S.; Van Der Wiel, W.G. Electrochemical Detection of Tumor-Derived Extracellular Vesicles on Nanointerdigitated Electrodes. *Nano Lett.* **2020**, *20*, 820–828. [CrossRef]
124. Kamath, R.; Madou, M.J. Selective Detection of Dopamine against Ascorbic Acid Interference Using 3D Carbon Interdigitated Electrode Arrays. *ECS Trans.* **2014**, *61*, 65. [CrossRef]
125. Rahimi, M.; Mikkelsen, S.R. Cyclic Biamperometry at Micro-Interdigitated Electrodes. *Anal. Chem.* **2011**, *83*, 7555–7559. [CrossRef]
126. Varshney, M.; Li, Y. Interdigitated array microelectrodes based impedance biosensors for detection of bacterial cells. *Biosens. Bioelectron.* **2009**, *24*, 2951–2960. [CrossRef]
127. Min, J.; Baeumner, A.J. Characterization and Optimization of Interdigitated Ultramicroelectrode Arrays as Electrochemical Biosensor Transducers. *Electroanalysis* **2004**, *16*, 724–729. [CrossRef]
128. Amato, L.; Keller, S.S.; Heiskanen, A.; Dimaki, M.; Emnéus, J.; Boisen, A.; Tenje, M. Fabrication of high-aspect ratio SU-8 micropillar arrays. *Microelectron. Eng.* **2012**, *98*, 483–487. [CrossRef]
129. Amato, L.; Heiskanen, A.; Hansen, R.; Gammelgaard, L.; Rindzevičius, T.; Tenje, M.; Emnéus, J.; Keller, S.S. Dense high-aspect ratio 3D carbon pillars on interdigitated microelectrode arrays. *Carbon* **2015**, *94*, 792–803. [CrossRef]
130. Han, M.; Lee, W.; Lee, S.-K.; Lee, S.S. Microfabrication of 3D oblique structures by inclined UV lithography. In *Micro Total Analysis Systems 2002*; Springer: Dordrecht, The Netherlands, 2002; pp. 106–108. [CrossRef]
131. Han, M.; Lee, W.; Lee, S.-K.; Lee, S.S. 3D microfabrication with inclined/rotated UV lithography. *Sens. Actuators A Phys.* **2004**, *111*, 14–20. [CrossRef]
132. Lee, J.B.; Choi, K.-H.; Yoo, K. Innovative SU-8 Lithography Techniques and Their Applications. *Micromachines* **2014**, *6*, 1–18. [CrossRef]
133. Del Campo, A.; Greiner, C. SU-8: A photoresist for high-aspect-ratio and 3D submicron lithography. *J. Micromech. Microeng.* **2007**, *17*, R81–R95. [CrossRef]
134. Lorenz, H.; Despont, M.; Fahrni, N.; Brugger, J.; Vettiger, P.; Renaud, P. High-aspect-ratio, ultrathick, negative-tone near-UV photoresist and its applications for MEMS. *Sens. Actuators A Phys.* **1998**, *64*, 33–39. [CrossRef]
135. Ganesh, E.N. Single walled and multi walled carbon nanotube structure, synthesis and applications. *Int. J. Innov. Technol. Explor. Eng.* **2013**, *2*, 311–320.
136. Brownlee, B.J.; Claussen, J.C.; Iverson, B.D. 3D Interdigitated Vertically Aligned Carbon Nanotube Electrodes for Electrochemical Impedimetric Biosensing. *ACS Appl. Nano Mater.* **2020**, *3*, 10166–10175. [CrossRef]
137. Lewis, P.M.; Sheridan, L.B.; Gawley, R.E.; Fritsch, I. Signal Amplification in a Microchannel from Redox Cycling with Varied Electroactive Configurations of an Individually Addressable Microband Electrode Array. *Anal. Chem.* **2010**, *82*, 1659–1668. [CrossRef]
138. Hong, F.; Cao, J.; Cheng, P. A parametric study of AC electrothermal flow in microchannels with asymmetrical interdigitated electrodes. *Int. Commun. Heat Mass Transf.* **2011**, *38*, 275–279. [CrossRef]
139. Sharma, D.; Lee, J.; Shin, H. An electrochemical immunosensor based on a 3D carbon system consisting of a suspended mesh and substrate-bound interdigitated array nanoelectrodes for sensitive cardiac biomarker detection. *Biosens. Bioelectron.* **2018**, *107*, 10–16. [CrossRef]
140. Bratov, A.; Abramova, N.; Marco, M.P.; Sanchez-Baeza, F. Three-Dimensional Interdigitated Electrode Array as a Tool for Surface Reactions Registration. *Electroanalysis* **2012**, *24*, 69–75. [CrossRef]
141. Han, D.; Kim, Y.-R.; Kang, C.M.; Chung, T.D. Electrochemical Signal Amplification for Immunosensor Based on 3D Interdigitated Array Electrodes. *Anal. Chem.* **2014**, *86*, 5991–5998. [CrossRef] [PubMed]
142. Jenkins, G.M.; Jenkins, A.; Kawamura, K. *Polymeric Carbons: Carbon Fibre, Glass and Char*; Cambridge University Press: Cambridge, UK, 1976.
143. Bose, A.; Sengupta, S. Fabrication and characterization of pillar interdigitated electrode for blood glucose sensing. *Sens. Rev.* **2021**, *41*, 200–207. [CrossRef]
144. Thivina, V.; Hashim, U.; Arshad, M.M.; Ruslinda, A.; Ayoib, A.; Nordin, N. Design and fabrication of Interdigitated Electrode (IDE) for detection of Ganoderma boninense. In Proceedings of the 2016 IEEE International Conference on Semiconductor Electronics (ICSE), Kuala Lumpur, Malaysia, 17–19 August 2016; pp. 50–53.
145. Mantis, I.; Hemanth, S.; Caviglia, C.; Heiskanen, A.; Keller, S.S. Suspended highly 3D interdigitated carbon microelectrodes. *Carbon* **2021**, *179*, 579–589. [CrossRef]
146. Lee, D.; Lee, S.; Rho, J.; Jang, W.; Han, S.H.; Chung, T.D. 3D interdigitated electrode array in the microchannel free of reference and counter electrodes. *Biosens. Bioelectron.* **2018**, *101*, 317–321. [CrossRef]
147. Brownlee, B.J.; Marr, K.M.; Claussen, J.C.; Iverson, B.D. Improving sensitivity of electrochemical sensors with convective transport in free-standing, carbon nanotube structures. *Sens. Actuators B Chem.* **2017**, *246*, 20–28. [CrossRef]
148. Marr, K.M.; Chen, B.; Mootz, E.J.; Geder, J.; Pruessner, M.; Melde, B.J.; Vanfleet, R.R.; Medintz, I.L.; Iverson, B.D.; Claussen, J.C. High aspect ratio carbon nanotube membranes decorated with Pt nanoparticle urchins for micro underwater vehicle propulsion via H_2O_2 decomposition. *ACS Nano* **2015**, *9*, 7791–7803. [CrossRef]
149. Lee, S.-J.; Anandan, V.; Zhang, G. Electrochemical fabrication and evaluation of highly sensitive nanorod-modified electrodes for a biotin/avidin system. *Biosens. Bioelectron.* **2008**, *23*, 1117–1124. [CrossRef]

150. Buzid, A.; Hayes, P.E.; Glennon, J.D.; Luong, J.H. Captavidin as a regenerable biorecognition element on boron-doped diamond for biotin sensing. *Anal. Chim. Acta* **2019**, *1059*, 42–48. [CrossRef]
151. Ding, S.; Das, S.R.; Brownlee, B.J.; Parate, K.; Davis, T.M.; Stromberg, L.R.; Chan, E.K.; Katz, J.; Iverson, B.D.; Claussen, J.C. CIP2A immunosensor comprised of vertically-aligned carbon nanotube interdigitated electrodes towards point-of-care oral cancer screening. *Biosens. Bioelectron.* **2018**, *117*, 68–74. [CrossRef]
152. Ohno, R.; Ohnuki, H.; Wang, H.; Yokoyama, T.; Endo, H.; Tsuya, D.; Izumi, M. Electrochemical impedance spectroscopy biosensor with interdigitated electrode for detection of human immunoglobulin A. *Biosens. Bioelectron.* **2013**, *40*, 422–426. [CrossRef]
153. Salinas-Torres, D.; Huerta, F.; Montilla, F.; Morallón, E. Study on electroactive and electrocatalytic surfaces of single walled carbon nanotube-modified electrodes. *Electrochim. Acta* **2011**, *56*, 2464–2470. [CrossRef]
154. Laureyn, W.; Van Gerwen, P.; Suls, J.; Jacobs, P.; Maes, G. Characterization of Nanoscaled Interdigitated Palladium Electrodes of Various Dimensions in KCl Solutions. *Electroanalysis* **2001**, *13*, 204–211. [CrossRef]
155. Banks, C.E.; Moore, R.R.; Davies, T.J.; Compton, R.G. Investigation of modified basal plane pyrolytic graphite electrodes: Definitive evidence for the electrocatalytic properties of the ends of carbon nanotubes. *Chem. Commun.* **2004**, 1804–1805. [CrossRef]
156. Banks, C.E.; Davies, T.J.; Wildgoose, G.G.; Compton, R.G. Electrocatalysis at Graphite and Carbon Nanotube Modified Electrodes: Edge-Plane Sites and Tube Ends Are the Reactive Sites. *ChemInform* **2005**, *36*, 241–829. [CrossRef]
157. 157. Dahlan, N.A.; Thiha, A.; Ibrahim, F.; Milić, L.; Muniandy, S.; Jamaluddin, N.F.; Petrović, B.; Kojić, S.; Stojanović, G. Role of Nanomaterials in the Fabrication of bioNEMS/MEMS for Biomedical Applications and towards Pioneering Food Waste Utilisation. *Nanomaterials* **2022**, *12*, 4025. [CrossRef]
158. Hasan, S. A review on nanoparticles: Their synthesis and types. *Res. J. Recent Sci.* **2015**, *2277*, 2502.
159. Tiwari, D.K.; Behari, J.; Sen, P. Application of nanoparticles in waste water treatment 1. *World Appl. Sci. J.* **2008**, *3*, 417–433.
160. Ealia, S.A.M.; Saravanakumar, M. A review on the classification, characterisation, synthesis of nanoparticles and their application. *IOP Conf. Ser. Mater. Sci. Eng.* **2017**, *263*, 032019. [CrossRef]
161. Salavati-Niasari, M.; Davar, F.; Mir, N. Synthesis and characterization of metallic copper nanoparticles via thermal decomposition. *Polyhedron* **2008**, *27*, 3514–3518. [CrossRef]
162. Daraee, H.; Eatemadi, A.; Abbasi, E.; Aval, S.F.; Kouhi, M.; Akbarzadeh, A. Application of gold nanoparticles in biomedical and drug delivery. *Artif. Cells Nanomed. Biotechnol.* **2014**, *44*, 410–422. [CrossRef] [PubMed]
163. Tran, H.-V.; Ngo, N.M.; Medhi, R.; Srinoi, P.; Liu, T.; Rittikulsittichai, S.; Lee, T.R. Multifunctional Iron Oxide Magnetic Nanoparticles for Biomedical Applications: A Review. *Materials* **2022**, *15*, 503. [CrossRef]
164. Manuja, A.; Kumar, B.; Kumar, R.; Chhabra, D.; Ghosh, M.; Manuja, M.; Brar, B.; Pal, Y.; Tripathi, B.; Prasad, M. Metal/metal oxide nanoparticles: Toxicity concerns associated with their physical state and remediation for biomedical applications. *Toxicol. Rep.* **2021**, *8*, 1970–1978. [CrossRef] [PubMed]
165. Waris, A.; Din, M.; Ali, A.; Afridi, S.; Baset, A.; Khan, A.U.; Ali, M. Green fabrication of Co and Co_3O_4 nanoparticles and their biomedical applications: A review. *Open Life Sci.* **2021**, *16*, 14–30. [CrossRef] [PubMed]
166. Singh, K.R.; Nayak, V.; Singh, J.; Singh, A.K.; Singh, R.P. Potentialities of bioinspired metal and metal oxide nanoparticles in biomedical sciences. *RSC Adv.* **2021**, *11*, 24722–24746. [CrossRef]
167. Fritea, L.; Banica, F.; Costea, T.O.; Moldovan, L.; Dobjanschi, L.; Muresan, M.; Cavalu, S. Metal Nanoparticles and Carbon-Based Nanomaterials for Improved Performances of Electrochemical (Bio)Sensors with Biomedical Applications. *Materials* **2021**, *14*, 6319. [CrossRef]
168. Sharma, D.; Lee, J.; Seo, J.; Shin, H. Development of a Sensitive Electrochemical Enzymatic Reaction-Based Cholesterol Biosensor Using Nano-Sized Carbon Interdigitated Electrodes Decorated with Gold Nanoparticles. *Sensors* **2017**, *17*, 2128. [CrossRef]
169. Nikolova, M.P.; Chavali, M.S. Metal Oxide Nanoparticles as Biomedical Materials. *Biomimetics* **2020**, *5*, 27. [CrossRef]
170. Nguyen, M.D.; Tran, H.-V.; Xu, S.; Lee, T.R. Fe_3O_4 Nanoparticles: Structures, synthesis, magnetic properties, surface functionalization, and emerging applications. *Appl. Sci.* **2021**, *11*, 11301. [CrossRef]
171. Aldeen, T.S.; Mohamed, H.E.A.; Maaza, M. ZnO nanoparticles prepared via a green synthesis approach: Physical properties, photocatalytic and antibacterial activity. *J. Phys. Chem. Solids* **2022**, *160*, 110313. [CrossRef]
172. Lingaraju, K.; Basavaraj, R.B.; Jayanna, K.; Bhavana, S.; Devaraja, S.; Swamy, H.M.K.; Nagaraju, G.; Nagabhushana, H.; Naika, H.R. Biocompatible fabrication of TiO_2 nanoparticles: Antimicrobial, anticoagulant, antiplatelet, direct hemolytic and cytotoxicity properties. *Inorg. Chem. Commun.* **2021**, *127*, 108505. [CrossRef]
173. Zhang, J.; Zhang, T.; Gao, J. Biocompatible Iron Oxide Nanoparticles for Targeted Cancer Gene Therapy: A Review. *Nanomaterials* **2022**, *12*, 3323. [CrossRef]
174. Stanicki, D.; Vangijzegem, T.; Ternad, I.; Laurent, S. An update on the applications and characteristics of magnetic iron oxide nanoparticles for drug delivery. *Expert Opin. Drug Deliv.* **2022**, *19*, 321–335. [CrossRef]
175. Luther, D.C.; Huang, R.; Jeon, T.; Zhang, X.; Lee, Y.-W.; Nagaraj, H.; Rotello, V.M. Delivery of drugs, proteins, and nucleic acids using inorganic nanoparticles. *Adv. Drug Deliv. Rev.* **2020**, *156*, 188–213. [CrossRef]
176. Tong, S.; Zhu, H.; Bao, G. Magnetic iron oxide nanoparticles for disease detection and therapy. *Mater. Today* **2019**, *31*, 86–99. [CrossRef]
177. Hola, K.; Markova, Z.; Zoppellaro, G.; Tucek, J.; Zboril, R. Tailored functionalization of iron oxide nanoparticles for MRI, drug delivery, magnetic separation and immobilization of biosubstances. *Biotechniol. Adv.* **2015**, *33*, 1162–1176. [CrossRef]

178. Baudler, A.; Schmidt, I.; Langner, M.; Greiner, A.; Schröder, U. Does it have to be carbon? Metal anodes in microbial fuel cells and related bioelectrochemical systems. *Energy Environ. Sci.* **2015**, *8*, 2048–2055. [CrossRef]
179. Saxena, U.; Das, A.B. Nanomaterials towards fabrication of cholesterol biosensors: Key roles and design approaches. *Biosens. Bioelectron.* **2016**, *75*, 196–205. [CrossRef]
180. Wiederoder, M.S.; Misri, I.; DeVoe, D.L. Impedimetric immunosensing in a porous volumetric microfluidic detector. *Sens. Actuators B Chem.* **2016**, *234*, 493–497. [CrossRef]
181. Taton, T.A.; Mirkin, C.A.; Letsinger, R.L. Scanometric DNA array detection with nanoparticle probes. *Science* **2000**, *289*, 1757–1760. [CrossRef]
182. Liu, R.; Feng, Z.-Y.; Li, D.; Jin, B.; Lan, Y.; Meng, L.-Y. Recent trends in carbon-based microelectrodes as electrochemical sensors for neurotransmitter detection: A review. *TrAC Trends Anal. Chem.* **2022**, *148*, 116541. [CrossRef]
183. Kucherenko, I.; Kucherenko, D.Y.; Soldatkin, O.; Lagarde, F.; Dzyadevych, S.; Soldatkin, A. A novel conductometric biosensor based on hexokinase for determination of adenosine triphosphate. *Talanta* **2016**, *150*, 469–475. [CrossRef]
184. Costas, A.; Florica, C.; Preda, N.; Besleaga, C.; Kuncser, A.; Enculescu, I. Self-connected CuO–ZnO radial core–shell heterojunction nanowire arrays grown on interdigitated electrodes for visible-light photodetectors. *Sci. Rep.* **2022**, *12*, 6834. [CrossRef] [PubMed]
185. Lee, S.; Nam, K.; Muhammad, W.; Shin, D.; Seo, S.; Kim, S.-D. Influence of N_2O plasma treatment on PET-based flexible bending sensors with ZnO nanorod array cross-linked with interdigitated electrode structures. *Ceram. Int.* **2022**, *48*, 25696–25704. [CrossRef]
186. Liu, F.; Tao, K.; Peiqi, D.; Shi, J. Photoelectrochemical oxygen evolution with interdigitated array electrodes: The example of TiO_2. *Nanotechnology* **2022**, *33*, 325701. [CrossRef] [PubMed]
187. Vahidpour, F.; Alghazali, Y.; Akca, S.; Hommes, G.; Schöning, M.J. An Enzyme-Based Interdigitated Electrode-Type Biosensor for Detecting Low Concentrations of H_2O_2 Vapor/Aerosol. *Chemosensors* **2022**, *10*, 202. [CrossRef]
188. Brosel-Oliu, S.; Chacón-Aparicio, S.; Ezenarro, J.J.; Abramova, N.; Uría, N.; Bratov, A. 3D Impedimetric Biosensor for Cyanobacteria Detection in Natural Water Sources. *Chemosensors* **2021**, *10*, 7. [CrossRef]
189. Ramanathan, S.; Gopinath, S.C.; Ismail, Z.H.; Arshad, M.M.; Poopalan, P. Aptasensing nucleocapsid protein on nanodiamond assembled gold interdigitated electrodes for impedimetric SARS-CoV-2 infectious disease assessment. *Biosens. Bioelectron.* **2022**, *197*, 113735. [CrossRef]
190. Srinivasan, K.P.; Muthuramalingam, T. Fabrication and Performance Evolution of AgNP Interdigitated Electrode Touch Sensor for Automotive Infotainment. *Sensors* **2021**, *21*, 7961. [CrossRef]
191. Bibi, A.; Rubio, Y.; Santiago, K.; Jia, H.-W.; Ahmed, M.; Lin, Y.-F.; Yeh, J.-M. H_2S-Sensing Studies Using Interdigitated Electrode with Spin-Coated Carbon Aerogel-Polyaniline Composites. *Polymers* **2021**, *13*, 1457. [CrossRef]
192. Wang, Y.; Du, H.; Xiao, D.; Zhang, Y.; Hu, F.; Sun, L. On-chip integration of bulk micromachined three-dimensional Si/C/CNT@TiC micro-supercapacitors for alternating current line filtering. *RSC Adv.* **2022**, *12*, 2048–2056. [CrossRef]
193. al Rumon, M.A.; Shahariar, H. Fabrication of interdigitated capacitor on fabric as tactile sensor. *Sens. Int.* **2021**, *2*, 100086. [CrossRef]
194. Tabei, H.; Morita, M.; Niwa, O.; Horiuchi, T. Fabrication and electrochemical features of new carbon based interdigitated array microelectrodes. *J. Electroanal. Chem.* **1992**, *334*, 25–33. [CrossRef]
195. Huang, X.-J.; O'Mahony, A.M.; Compton, R.G. Microelectrode Arrays for Electrochemistry: Approaches to Fabrication. *Small* **2009**, *5*, 776–788. [CrossRef]
196. Fiaccabrino, G.; Tang, X.-M.; Skinner, N.; De Rooij, N.; Koudelka-Hep, M. Electrochemical characterization of thin-film carbon interdigitated electrode arrays. *Anal. Chim. Acta* **1996**, *326*, 155–161. [CrossRef]
197. Niwa, O.; Horiuchi, T.; Tabei, H. Electrochemical properties of carbon based interdigitated microarray electrodes fabricated by the pyrolysis of electrochemically prepared conducting films. *J. Electroanal. Chem.* **1994**, *367*, 265–269. [CrossRef]
198. Mamishev, A.; Sundara-Rajan, K.; Yang, F.; Du, Y.; Zahn, M. Interdigital sensors and transducers. *Proc. IEEE* **2004**, *92*, 808–845. [CrossRef]
199. Rassaei, L.; Singh, P.S.; Lemay, S.G. Lithography-Based Nanoelectrochemistry. *Anal. Chem.* **2011**, *83*, 3974–3980. [CrossRef]
200. Hassan, Y.; Caviglia, C.; Hemanth, S.; Mackenzie, D.; Alstrøm, T.; Petersen, D.; Keller, S. High temperature SU-8 pyrolysis for fabrication of carbon electrodes. *J. Anal. Appl. Pyrolysis* **2017**, *125*, 91–99. [CrossRef]
201. Hassan, Y.M.; Caviglia, C.; Hemanth, S.; Mackenzie, D.M.A.; Petersen, D.H.; Keller, S.S. Pyrolytic carbon microelectrodes for impedance based cell sensing. *ECS Trans.* **2016**, *72*, 35–44. [CrossRef]
202. Pu, Q.; Yun, J.; Temkin, A.H.; Liu, S. Ion-Enrichment and Ion-Depletion Effect of Nanochannel Structures. *Nano Lett.* **2004**, *4*, 1099–1103. [CrossRef]
203. Stein, D.; Kruithof, M.; Dekker, C. Surface-Charge-Governed Ion Transport in Nanofluidic Channels. *Phys. Rev. Lett.* **2004**, *93*, 035901. [CrossRef] [PubMed]
204. Sharma, D.; Lim, Y.; Lee, Y.; Shin, H. Glucose sensor based on redox-cycling between selectively modified and unmodified combs of carbon interdigitated array nanoelectrodes. *Anal. Chim. Acta* **2015**, *889*, 194–202. [CrossRef] [PubMed]
205. Uda, M.N.A.; Gopinath, S.C.B.; Hashim, U.; Hakimi, A.; Anuar, A.; A A Bakar, M.; Sulaiman, M.K.; A Parmin, N. Harumanis Mango: Perspectives in Disease Management and Advancement using Interdigitated Electrodes (IDE) Nano-Biosensor. *IOP Conf. Ser. Mater. Sci. Eng.* **2020**, *864*, 012180. [CrossRef]

206. Li, W.; Liu, G.; Jiang, D.; Wang, C.; Li, W.; Guo, T.; Zhao, J.; Xi, F.; Liu, W.; Zhang, C. Interdigitated Electrode-Based Triboelectric Sliding Sensor for Security Monitoring. *Adv. Mater. Technol.* **2018**, *3*, 1800189. [CrossRef]
207. Kanade, P.P.; Oyunbaatar, N.-E.; Lee, D.-W. Polymer-Based Functional Cantilevers Integrated with Interdigitated Electrode Arrays—A Novel Platform for Cardiac Sensing. *Micromachines* **2020**, *11*, 450. [CrossRef]